



# **Modelling Isoprene Emissions over Southern Africa Based on Climate Change Scenarios**

Michael John Weston

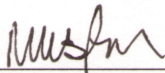
A dissertation submitted to the Faculty of Science, University of the Witwatersrand, Johannesburg, in fulfillment of the requirements for the degree of Master of Science.

February 2011

## DECLARATION

I declare that this dissertation is my own, unaided work, except where otherwise stated. It is being submitted for the degree of Master of Science in the University of the Witwatersrand, Johannesburg. It has not been submitted before for any degree or examination in any other university.

Signed this 11 day of October 2011



---

Michael John Weston.

## ABSTRACT

Biogenic volatile organic compounds (BVOCs), in the presence of nitrogen oxide gases ( $\text{NO}_x$ ), play a role in the production of tropospheric ozone ( $\text{O}_3$ ) which is an effective greenhouse gas and is hazardous to human health (Haagen-Smit, 1952, Chameides *et al*, 1988, Atkinson, 2000, Kanakidou *et al*, 2004). Isoprene is a single BVOC that accounts for over 50% of all emitted BVOCs. Isoprene emissions are species specific and vary according to temperature, light and leaf area index. Climate change studies predict that the geographic distribution of species, temperature ranges, light intensity and leaf area index will shift, thus altering future isoprene emissions.

Several attempts to model BVOC emissions have been undertaken in an effort to quantify BVOC emission rates and the impact on ozone formation. The most widely used and empirically tested emission algorithms to date were developed by Guenther *et al* (1993) and are incorporated into the emission model Model of Emissions of Gases and Aerosols from Nature (MEGAN). MEGAN is used in this study to model isoprene emission rates over southern Africa under current and future climate conditions. Current and future climate conditions are taken from the regional climate model, Conformal-Cubic Atmospheric Model (C-CAM), which has been shown to simulate current climate well for the region. Emissions were modelled for January and July only, to represent summer and winter conditions.

January isoprene emission rates for the current climate range from 0 to  $1.41 \text{ gm}^{-2}\text{month}^{-1}$  and total 0.938 Tg of isoprene for the study domain. The highest emission rates are caused by combinations of driving variables which are: high temperature only; high temperature and high leaf area index; high emission factor and high leaf area index. Emission rates effectively shut down in July due to low temperatures and low leaf area index. July emission rates range from 0 to  $0.61 \text{ gm}^{-2}\text{month}^{-1}$  and total 0.208 Tg of isoprene. Temperature is shown to cause the greatest variation in isoprene emission rates, and thus future scenarios represent an increase in temperature only. The spatial distribution of future emission rates does not shift when compared to current emission rates, but does show an increase in magnitude. Future emission totals for January increase

by 34% to 1.259 Tg of isoprene and the July emission total increases by 38% to 0.289 Tg of isoprene.

Future emission rates responded to temperature as expected, increasing in magnitude, rate of change and range of temperature over which the greatest rate of change occurs. Three areas demonstrating the highest increase in emission rates and highest future emission rates were identified. As temperature was the only variable altered in future scenarios, these areas can be deemed as areas most sensitive to changes in temperature. These areas are situated near the Angola-Namibia border, the Northern Interior of South Africa and the low-lying areas of Mozambique.

*This dissertation is dedicated to my parents*

*Nadine Gwenneth Weston*

*and*

*Derek William John Weston*

## PREFACE

Biogenic volatile organic compounds (BVOCs) are emitted from vegetation and have been shown to play a role in tropospheric ozone formation. Ozone is an efficient greenhouse gas and is hazardous to human health. Emission models have been developed in an effort to quantify BVOC emissions and their associated role in ozone formation. These models are based on the driving variables of BVOC emission rates like tree species distribution, leaf temperature, light intensity and leaf area index. These driving variables are expected to change over the next 70 to 100 years, which is the same time scale as climate change models. Consequently, BVOC emission models have been used to determine current emission rates and make use of climate change models to provide the first step in estimating future emission rates and associated impacts on future ozone formation.

Global emission models have been used to estimate future BVOC emissions using temperature and light data from General Circulation Models (GCMs). However, GCM data is typically at a coarse resolution of about 1° longitude by 1° latitude. BVOCs have been modelled over southern Africa at a resolution of 1km using observed data for the year 2003, but no modelling has been conducted for a future scenario at high resolution. The objective of this study is to model BVOC emissions over southern Africa for the current and future climate using dynamically downscaled GCM data at a resolution of about 0.5°. The aims include:

- Identifying areas with high isoprene emissions.
- Identify the driving variable/s of isoprene emissions over these areas.
- Verify that emissions are sensitive to temperature as expected.
- Identify areas that are most affected by temperature sensitivity.

This dissertation is divided into five chapters. Chapter 1 provides background information relating the BVOCs and atmospheric chemistry, the importance of isoprene as a BVOC, emission modelling, climate change modelling and the relationship between

BVOC emission rates and their driving variables. Chapter 2 provides a description of the emission model MEGAN and the data sets used. The results for the current climate are presented in Chapter 3 and the validity of the modelled emission rates is assessed. Emission rates under future conditions are presented in Chapter 4 and an assessment is made of emission rate sensitivity to temperature. Chapter 5 offers a summary and some conclusions.

Prof. Stuart Piketh provided me with many opportunities during my MSc for which I am very grateful. These include a visit to NCAR to learn how to run MEGAN, working on local and international projects and attending local and international conferences. He also provided most of the funding and always offered pertinent comments after reading draft copies. Funding was also provided through the Wits post graduate merit award for part of my studies.

Roelof Burger was an endless source of ideas and assistance during this project. Without him this work would not have been possible. His assistance added much value to this research and is greatly appreciated.

Thank you to Dr. Luanne Otter for providing guidance on the initial scope and methodology of this project.

Thank you to my parents for supporting what seemed like a professional student! Lastly, thank you to my fellow students at the Climatology Research Group for being a constant source of entertainment and moral support.

## List of abbreviations

BVOC	Biogenic Volatile Organic Compound
C-CAM	Conformal-Cubic Atmospheric Model
DPPFD	Daily Average Photosynthetic Photon Flux Density
GCM	General Circulation Model
LAI	Leaf Area Index
MEGAN	Model of Emissions of Gases and Aerosols from Nature
PAC	Above Canopy Photosynthetic Active Radiation
PAR	Photosynthetic Active Radiation
PPFD	Photosynthetic Photon Flux Density
RCM	Regional Circulation Model
VOC	Volatile Organic Compound



## CONTENTS

DECLARATION .....	II
ABSTRACT .....	III
PREFACE .....	VI
CONTENTS .....	IX
CHAPTER 1 : OVERVIEW .....	12
Introduction .....	12
Volatile Organic Compounds and Atmospheric Chemistry .....	13
Biogenic VOCs .....	14
Importance of BVOCs in Chemistry Modelling .....	15
Ozone Formation through Photo-dissociation .....	15
Hydrogen Abstraction Reaction: Formation of Ozone from BVOCs .....	16
Alkene-OH Reaction .....	17
Ozone Destruction .....	18
Diurnal Cycle of Ozone Concentrations .....	20
Existing BVOC Estimates over Southern Africa .....	21
Calculating Emission Estimates .....	22
Importance of Isoprene as a BVOC .....	22
Temperature Dependence of Isoprene .....	23
Light Dependence of Isoprene .....	24
Relevance on Future Emission Estimates of Isoprene .....	24
Land Cover Change .....	25
Future Temperatures .....	26
Changes in Radiation .....	26
Effect of Elevated CO <sub>2</sub> .....	26
Estimating Future Temperatures Using a Regional Climate Model .....	27
Predicting Future Scenarios of Temperature Increase using General Circulation Models .....	28
The Conformal-Cubic Atmospheric Model .....	29
Estimating Emissions using an Emissions Model .....	29
Model Inputs .....	30
Emission factor .....	30
Emission Activities .....	31
Leaf Area Index .....	31
Emission Activity and Model Uncertainty .....	31
Temperature produces the most uncertainty .....	32
Summary and Objectives .....	36
CHAPTER 2 : DATA AND METHODOLOGY .....	37
Overview of MEGAN .....	37
MEGAN Algorithms .....	38
A Brief Explanation on Interpreting Model Outputs .....	41
Contribution of Model Inputs in Calculating Model Output .....	41
Identifying Driving Variables of Isoprene Emissions .....	41

Installing the MEGAN Software .....	42
Running MEGAN .....	42
Input Land Cover Data.....	43
Defining the MEGAN Model Domain .....	43
Isoprene Emission Factor Input Data.....	43
Leaf Area Index (LAI) Input Data .....	44
Calculating Isoprene Emission Rates.....	46
Input Temperature Data .....	46
Input Light Data.....	47
Error with Data Time Stamps .....	48
Processing MEGAN output .....	49
Quantitative versus Qualitative Methods in Representing Model Uncertainty .....	50
Identifying Areas of 'High' Emission Rates.....	51
<b>CHAPTER 3 : ISOPRENE EMISSIONS OVER SOUTHERN AFRICA BASED ON</b>	
<b>CURRENT CLIMATE CONDITIONS.....</b>	<b>52</b>
Spatial Distribution of CURRENT Isoprene Emission Rate Estimates.....	52
January CURRENT .....	52
Driving Variables of Peak Isoprene Emissions .....	53
July CURRENT .....	55
Comparison of Spatial Distribution of CURRENT Isoprene Emission Rates with a	
Previous Study .....	57
Magnitude of CURRENT Isoprene Emission Rates.....	58
Range of Isoprene Emission Rates in Comparison to Previous Studies.....	58
Total Isoprene Emitted over the Study Domain .....	59
Range of Emission Activity in Comparison to Previous Studies .....	60
Precautions to Consider when Comparing Independent Model Studies.....	61
<b>CHAPTER 4 : SENSITIVITY ANALYSIS OF ISOPRENE EMISSIONS TO</b>	
<b>TEMPERATURE USING CLIMATE CHANGE SCENARIOS.....</b>	<b>64</b>
Introduction.....	64
Future Temperature Scenarios .....	64
Spatial Distribution of FUTURE Isoprene Emission Rates.....	65
Regional Totals of Isoprene Emissions and Percent Increase for CURRENT and	
FUTURE .....	66
Percentage Increase in Isoprene Emission Rates .....	68
Sensitivity of Isoprene Emissions to Temperature .....	68
Do Emissions Respond to Temperature as Expected?.....	68
Areas demonstrating high isoprene emission rates and sensitivity to temperature ..	74
Other Factors that may affect Sensitivity.....	76
Leaf Area Index .....	76
Changing Emission Factors due to Changing Land Cover.....	77
Summary .....	78
<b>CHAPTER 5 : SUMMARY AND CONCLUSIONS.....</b>	<b>79</b>
Areas of Highest Isoprene Emissions and Associated Driving Variables .....	79
Sensitivity of Isoprene Emissions to Increases in Temperature .....	80
The Use of a Regional Climate Model in Estimating Isoprene Emissions.....	81

REFERENCES ..... 82

## CHAPTER 1: OVERVIEW

This chapter highlights the role of biogenic volatile organic compounds (BVOCs) in atmospheric chemistry, emphasizing ozone formation as a final product. Consequently, efforts to quantify BVOC emissions have made use of emission models to determine the impact of BVOCs on atmospheric chemistry. Emission models have been run at coarse resolution for global studies and finer resolution for regional studies. Emission estimates from such models will be presented. The driving forces of BVOC emissions will be discussed, with reference to how they are included in an emission model called Model of Emissions of Gases and Aerosol from Nature (MEGAN). Motivation is given for the study of a single BVOC called isoprene. An argument is made that driving forces of isoprene emissions will change over timescales similar to climate change predictions and thus future isoprene emission estimates are required. Finally, a sensitivity analysis of the MEGAN model is discussed, showing how changes in driving variables affect the final emission rate.

### Introduction

Biogenic volatile organic compounds (BVOCs) are emitted from vegetation and have been shown to play a role in tropospheric ozone formation (Haagen-Smit, 1952, Chameides *et al*, 1988, Atkinson, 2000, Kanakidou *et al*, 2004). Ozone is an efficient greenhouse gas and is hazardous to human health. Emission models have been developed in an effort to quantify BVOC emissions and their associated role in ozone formation. These models are based on the driving variables of BVOC emission rates like tree species distribution, leaf temperature, light intensity and leaf area index. These driving variables are expected to change over the next 70 to 100 years, which is the same timescale as climate change models. Consequently, BVOC emission models have been used to determine current emission rates and make use of climate change models to provide the first step in estimating future emission rates and associated impacts on future ozone

formation. This dissertation presents results from a BVOC emissions model that was run over southern Africa for current and future climate scenarios.

### **Volatile Organic Compounds and Atmospheric Chemistry**

Volatile organic compounds (VOCs), in the presence of nitrogen oxide gases ( $\text{NO}_x$ ), play a role in the production of tropospheric ozone ( $\text{O}_3$ ) and in the formation of secondary aerosols (Haagen-Smit, 1952, Chameides *et al*, 1988, Atkinson, 2000, Kanakidou *et al*, 2004). Both ozone and aerosols alter the earth's radiation balance and are detrimental to human health. Furthermore, VOCs strongly effect hydroxyl (OH) concentrations which influence methane ( $\text{CH}_4$ ) and carbon monoxide (CO) concentrations (Guenther *et al*, 1995). Consequently, VOCs indirectly affect the concentrations of the greenhouse gases  $\text{O}_3$  and  $\text{CH}_4$  and radiatively active aerosols.

As a greenhouse gas, tropospheric  $\text{O}_3$  is the third highest contributor to atmospheric warming after carbon dioxide ( $\text{CO}_2$ ) and methane. Global annual mean estimates of radiative forcing for tropospheric  $\text{O}_3$ ,  $\text{CO}_2$  and  $\text{CH}_4$  are 0.35, 1.46 and 0.48  $\text{Wm}^{-2}$  respectively (IPCC, 2001). However, emissions of precursors to ozone formation, particularly  $\text{NO}_x$  gases, are expected to increase in the future. Consequently, the contribution of ozone to atmospheric warming may increase. Thus, it is important to quantify all precursors to ozone formation under future scenarios, including VOC emissions. Furthermore, ozone is a strong oxidizing agent, and consequently causes damage to biological cells. This has a detrimental affect on human health, particularly affecting the lining of the lungs (Chen *et al*, 2007, Berry *et al*, 1991, Lippmann, 1989). Damage to the lining of the lungs increases risk to pathogens and increases inflammation of the airways. Short term affects of ozone include shortness of breath, coughing and chest pains. However, long term exposure and damage can lead to a permanent decrease in lung capacity and heart conditions.

The radiative effect of aerosols is much more challenging to quantify than for trace gases like ozone. Aerosols, or particulate matter, differ in size, chemical composition and spatial distribution. The size of the particle determines how much radiation is scattered, while the chemical composition determines whether radiation is absorbed or not (IPCC,

2001). Consequently, aerosols could either cool the atmosphere through scattering radiation or heat the atmosphere by absorbing radiation. Furthermore, aerosols can have a secondary affect on radiation by altering the characteristics of clouds, causing clouds to become long-lived and therefore, altering the radiation balance (Twomey, 1977). Aerosols affect health by entering the lungs and causing similar symptoms to exposure to ozone. Symptoms are similar because, like ozone, aerosols cause agitation in the lung lining, resulting in coughing, inflammation and narrowing of the airways (Davidson *et al*, 2005, Seaten *et al*, 1995, McKee, 1993). As VOCs act as a source of aerosol formation, estimates of VOC emissions are required to help quantify current and future aerosol concentrations.

VOCs are emitted from both anthropogenic and natural sources. Anthropogenic sources include combustion and storage of fossil fuels, industrial processes, waste treatment and agricultural activity (Muller, 1992, Piccot *et al.*, 1992, Friedrich and Obermeier, 1999). Initially, attention was brought to VOCs when it was found that they are associated with ozone formation in photochemical smog over urban areas (Haagen-Smit, 1952). Thus, early ozone abatement strategies included plans to decrease VOC emissions from anthropogenic sources (Chameides *et al*, 1988). However, studies have since shown that biogenic emissions play just as important a role in atmospheric chemistry and ozone formation (Guenther *et al*, 1999a).

### **Biogenic VOCs**

Biogenic VOCs (BVOC) are emitted from vegetation and account for 90 % of the VOCs emitted by natural sources, which includes oceans and soil (Guenther *et al*, 1995). Total emissions from biogenic sources are estimated at  $1150 \text{ TgC yr}^{-1}$ , which is seven times higher than emissions from anthropogenic sources (Guenther *et al*, 1995, Guenther *et al*, 1999a). Although this comparison does not represent the relative source strength or emission rates from biogenic and anthropogenic sources, it does illustrate the relative importance of BVOCs in terms of total VOCs emitted. The effect of these higher emissions on ozone formation is best demonstrated using atmospheric chemistry models.

### **Importance of BVOCs in Chemistry Modelling**

Atmospheric chemistry models demonstrate that BVOCs require  $\text{NO}_x$  gases in order to contribute to  $\text{O}_3$  formation. Trainer *et al* (1987) used a chemistry model to determine ozone concentration depending on various emission scenarios. Model inputs were determined from field measurements and the model was run for three scenarios. As  $\text{NO}_x$  and VOCs are precursors to  $\text{O}_3$  formation, the first scenario modelled  $\text{NO}_x$  emissions with zero BVOC and anthropogenic VOC emissions. The second scenario included BVOC emissions and the third included BVOC and anthropogenic VOC emissions. Results showed that after BVOCs were added,  $\text{O}_3$  concentrations increased strongly. In the absence of  $\text{NO}_x$ , as was the case for some areas in the model, BVOCs contributed little to  $\text{O}_3$  formation. In a similar study, Thunis and Cuvelier (2000) found that a reduction in  $\text{O}_3$  formation was not due to a decrease in BVOCs, but a decrease in  $\text{NO}_x$  concentrations. This indicates that the effect of BVOCs on ozone formation is dependent on  $\text{NO}_x$  concentrations. Chameides *et al* (1988) found that, after removing anthropogenic emissions from the model, BVOC concentrations were still high enough to produce ozone concentrations that exceeded the national ambient air quality standard of 0.12 ppmv. All three cases show that BVOCs, in the presence of  $\text{NO}_x$ , contribute to ozone formation.

The relationship between BVOCs and  $\text{O}_3$  is complex and involves many reaction pathways. The time of day, along with relative concentrations of  $\text{NO}_x$  gases, determines whether  $\text{O}_3$  formation or destruction is favoured. As a result, increases in BVOC concentration do not result in a linear increase in  $\text{O}_3$ , as will be discussed later in this section. Some of the major reaction pathways will be discussed here, highlighting important chemical compounds in  $\text{O}_3$  formation. These, along with reaction rates and less common reaction pathways, are all taken into account when determining  $\text{O}_3$  concentrations in atmospheric chemistry models.

#### *Ozone Formation through Photo-dissociation*

The major  $\text{O}_3$  forming pathway is the photo-dissociation of  $\text{NO}_2$



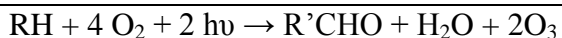
BVOCs affect this reaction cycle in two ways. Firstly, BVOCs react with hydroxyl radicals (OH) and nitrogen oxide (NO) to form NO<sub>2</sub> which in turn forms O<sub>3</sub>. Secondly, because BVOCs react with NO, they are in competition with O<sub>3</sub> for NO. As a result, BVOCs can limit the breakdown of O<sub>3</sub> represented in reaction (R3) and effectively increase O<sub>3</sub> concentrations.

#### *Hydrogen Abstraction Reaction: Formation of Ozone from BVOCs*

BVOCs are oxidised through a series of reactions known as the photochemical smog mechanism or hydrogen abstraction reaction (Volz-Thomas *et al.* 1997). The net result of these reactions is the production of two NO<sub>2</sub> molecules, which form two ozone molecules, from one BVOC molecule. The first reaction in the series is between a reactive hydrocarbon (RH), or BVOC, and a hydroxyl radical (OH). The product of this reaction reacts with oxygen almost immediately to produce a peroxy radical (RO<sub>2</sub>). Peroxy radicals are important in this reaction series as they react with NO to form NO<sub>2</sub>. The reactive oxygen atom in the peroxy radical reacts with NO to form the first NO<sub>2</sub> (R6). The by-product of the peroxy radical-NO reaction reacts with O<sub>2</sub> to form another peroxy radical, HO<sub>2</sub> (R7). This peroxy radical, like the previous one, also reacts with NO to form the second NO<sub>2</sub>. Further peroxy radicals can be produced through minor pathways which degrade the aldehyde, R'CHO, produced in (R7). The reaction series discussed above involves hydrogen abstraction to form H<sub>2</sub>O in the initial step (R1). However, if the VOC is an alkene, as most are (Seinfeld and Pandis, 1998), a similar series of reactions can occur via the addition of OH to the double bond ((R11) to (R16)).

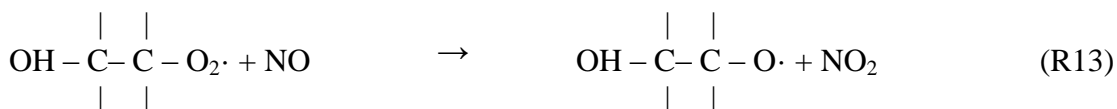
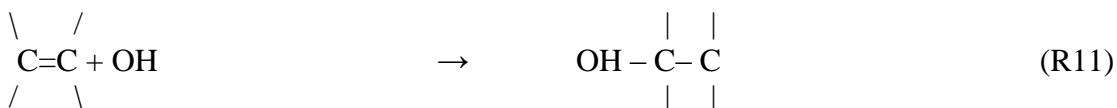


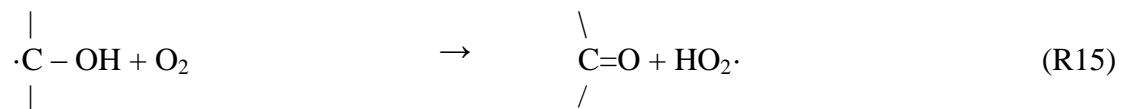
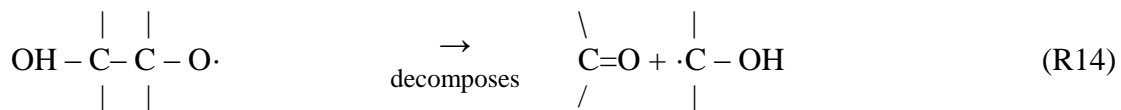




### *Alkene-OH Reaction*

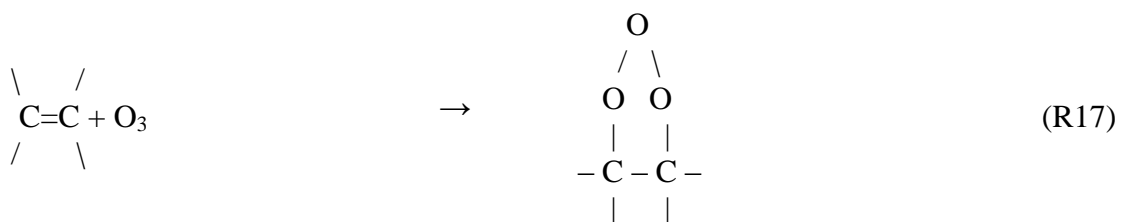
The alkene-OH reaction is essentially the same as the hydrogen abstraction reaction: one VOC molecule oxidised in the presence of NO produces two NO<sub>2</sub> molecules that then produce two O<sub>3</sub> molecules. As in the hydrogen abstraction reaction, the alkene-OH reaction produces a peroxy radical which reacts with NO to form the first NO<sub>2</sub>. The alkene-OH reaction now includes an extra reaction. After the peroxy radical reacts with NO, another radical is formed that decomposes before reacting with O<sub>2</sub>. Decomposition produces a formaldehyde molecule and another radical that then reacts with O<sub>2</sub> (R14). The reaction of this radical with O<sub>2</sub> produces another formaldehyde molecule as well as a hydroperoxyl radical (peroxy radical) (HO<sub>2</sub>) (R15). The hydroperoxyl radical then reacts with NO to form the second NO<sub>2</sub> (R16). Although peroxy radicals can react with compounds other than NO, the reaction with NO is the major pathway (Seinfeld and Pandis, 1998). There is no net loss of the OH radical as it is reproduced in the final reaction. Thus, the series of reactions are able to start again.



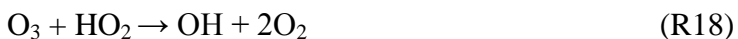


### Ozone Destruction

The major compounds involved in O<sub>3</sub> formation, VOCs, OH, peroxy radicals and NO, can also react with O<sub>3</sub>, effectively decreasing concentrations. Ozone can react with the double bond in alkenes to produce an ozonide (R17). The ozonide then decomposes into chemical compounds, a carbonyl and a biradical, that are not used in any of the O<sub>3</sub> forming reactions (Seinfeld and Pandis, 1998).



Ozone also reacts with the hydroperoxyl radical and the hydroxyl radical, effectively decreasing O<sub>3</sub> concentrations ((R18) and (R19)) (Volz-Thomas *et al*, 1997).



Finally, ozone decreases due to photolysis (Dickerson *et al*, 1982, Volz-Thomas *et al*, 1997). Ozone photolysis requires light with wavelengths less than 320nm. This is ultra violet light and more specifically biologically active solar UV light (UVB) (Dickerson *et al*, 1982). Photolysis is more important with regard to stratospheric ozone, as this is

where most of the UV light is absorbed. Tropospheric ozone is more likely to be destroyed via chemical reactions than photolysis. Ozone photolysis usually produces an oxygen atom that then reacts with water to form a hydroxyl radical ((R20) and (R21)).



If we are to determine which reactions will predominate we need to consider the speed of the reactions (Table 1.1). Reaction rate constants in Table 1.1 are given in decreasing order. Reactions with higher reaction rates will occur faster and are more likely to predominate in atmospheric conditions. It must be noted that the reactions in Table 1.1 are limited by the availability of the primary chemical species in the reaction. Thus, although the reaction may occur quickly, it may not be as important as other reactions as the concentrations of the primary compounds may be lower than for other reactions. Reactions that belong to the series of ozone forming reactions have the fastest reaction rates (reactions 4 and 5). Reactions that involve ozone destruction (reactions 6-13) are at least an order of magnitude slower than ozone forming reactions. This suggests therefore that under day time atmospheric conditions ozone forming reactions are more likely to dominate.

Table 1.1: Reaction rate constants in decreasing order for major ozone reactions.

	Reaction	Rate Constant <sup>a</sup> (cm <sup>3</sup> molecule <sup>-1</sup> s <sup>-1</sup> )	Time of importance <sup>b</sup>	References
1	$\text{NO}_2 + h\nu \rightarrow \text{NO} + \text{O}$	Depends on light intensity	Day	Seinfeld and Pandis, 1998
2	$\text{O} + \text{O}_2 + \text{M} \rightarrow \text{O}_3 + \text{M}$ (three body reaction)	$6.0 \times 10^{-34}$ (cm <sup>6</sup> molecule <sup>-2</sup> s <sup>-1</sup> )	Day	Seinfeld and Pandis, 1998
3	$\text{O}_3 + h\nu \rightarrow \text{O}_2 + \text{O} (^1\text{D})$ Photodissociation. Occurs in stratosphere.	Depends on light intensity	Day	Seinfeld and Pandis, 1998
4	$\text{RH} + \text{OH} \rightarrow \text{RO}_2 + \text{H}_2\text{O}$ H-extraction	$2.63 \times 10^{-11}$	Day	Seinfeld and Pandis, 1998
5	$\text{NO} + \text{HO}_2 \rightarrow \text{NO}_2 + \text{OH}$	$8.6 \times 10^{-12}$	Day	Seinfeld and Pandis, 1998
6	$\text{NO}_2 + \text{O}_3 \rightarrow \text{NO}_3 + \text{O}_2$	$1.4 \times 10^{-13}$	Day	Pienaar and Helas, 1996

7	$\text{OH} + \text{O}_3 \rightarrow \text{HO}_2 + \text{O}_2$	$6.8 \times 10^{-14}$	Day	Seinfeld and Pandis, 1998
8	$\text{NO} + \text{O}_3 \rightarrow \text{NO}_2 + \text{O}_2$	$1.8 \times 10^{-14}$	Day	Seinfeld and Pandis, 1998
9	$\text{NO} + \text{O}_3 \rightarrow \text{NO}_2 + \text{O}_2$	$1.8 \times 10^{-14}$	Night	Seinfeld and Pandis, 1998
10	$\text{HO}_2 + \text{O}_3 \rightarrow \text{OH} + 2\text{O}_2$	$2.0 \times 10^{-15}$	Night	Seinfeld and Pandis, 1998
11	$\text{NO}_2 + \text{O}_3 \rightarrow \text{NO}_3 + \text{O}_2$	$3.2 \times 10^{-17}$	Night	Seinfeld and Pandis, 1998
12	Isoprene + $\text{O}_3 \rightarrow$ Products	$1.19 \times 10^{-17}$		Klawatsch-Carrasco <i>et al</i> , 2004
13	MBO* + $\text{O}_3 \rightarrow$ Products	$8.3 \times 10^{-18}$		Klawatsch-Carrasco <i>et al</i> , 2004

<sup>a</sup> Rate constants from Seinfeld and Pandis, 1998 are at 298 K.  
Rate constants for Klawatsch-Carrasco *et al*, 2004 are at 293±2 K

<sup>b</sup> Time of importance was only given in Pienaar and Helas, 1996, not in Seinfeld and Pandis, 1998.

\* MBO is 2-methyl-3-buten-2-ol

### *Diurnal Cycle of Ozone Concentrations*

As we have seen, the chemistry of ozone production is very complex. Ozone, VOCs and NO<sub>x</sub> gases interact in a way that makes it almost impossible to consider each compound's chemistry separately. However, we may understand the complexity better if we consider characteristic diurnal and nocturnal concentrations.

The diurnal pattern is governed mainly by light. During the day, VOCs and ozone both increase in concentration. BVOC emissions increase because they are temperature and light dependent (Monson *et al*, 1992, Sharkey *et al*, 1996, Harley *et al*, 1996, Harley *et al*, 1997, Singaas and Sharkey, 2000) and ozone increases due to photolysis of NO<sub>2</sub> (Table 1.1). NO<sub>2</sub> photolysis requires a low activation energy and is activated by visible light (usually violet) or any wavelength less than 420nm (Dickerson *et al*, 1982). Thus NO<sub>2</sub> decreases. At night there is usually a reverse in these trends. VOCs and ozone decrease while NO<sub>2</sub> increases because it is no longer broken down by photolysis. To understand the chemistry involved we need to consider the hydroxyl radical (OH).

VOCs and NO<sub>x</sub> compete for OH. This competition determines the rate of ozone production. Seinfeld and Pandis (1998) suggest that for an 'average urban mix' of NO<sub>x</sub>

and VOCs the rate constant for the OH-NO<sub>2</sub> reaction is 5.5 times faster than the OH-VOC reaction (on a per carbon atom basis). Therefore, VOC concentrations need to be 5.5 times higher than NO<sub>x</sub> concentrations to compete equally for the OH. Any variation above or below this ratio will result in increased or decreased ozone production. A high ratio will occur during the day when VOC emissions are highest (Trainer *et al*, 1987, Monson *et al*, 1992, Sharkey *et al*, 1996, Harley *et al*, 1996, Harley *et al*, 1997). This promotes ozone production. VOCs will compete for the OH, oxidise and form peroxy radicals. Peroxy radicals then react with NO<sub>x</sub> gases to form ozone. However, if NO<sub>x</sub> concentrations become very low, they will not react with peroxy radicals. Peroxy-peroxy reactions will take place and ozone will not be produced. Even though the ratio is higher here, ozone production will become limited. When the ratio is lower (VOCs decrease), OH will react mainly with NO<sub>x</sub> gases, therefore limiting ozone formation. This is most likely to occur at night when BVOC emissions almost stop and there is no photo dissociation of NO<sub>x</sub> gases.

### **Existing BVOC Estimates over Southern Africa**

Initially, studies presented emission estimates of BVOCs over southern Africa as part of total global emission estimates (Guenther *et al*, 1995, Guenther *et al*, 1999a). The major drawback associated with calculating global emission estimates is collecting data for a large area. Data is often represented at a large, or coarse, scale and detail is lost. As an alternative, regional studies can be conducted, allowing for more time and effort to be spent on determining more detailed spatial distribution of emission estimates. The first study to represent BVOC emission estimates over Africa south of the Equator at a spatial scale of 1 km was conducted by Otter *et al* (2003). Total BVOC emissions were calculated at 80 Tg C yr<sup>-1</sup>. Estimates from this study were later used as input into an atmospheric chemistry model (CAMx) to estimate ozone concentrations over the region (Zunckel *et al*, 2006).

Zunckel *et al* (2006) found that biogenic precursors contributed to ozone formation. Other input data in the CAMx study included anthropogenic NO<sub>x</sub> and VOC sources and NO<sub>x</sub> emissions from soil. Anthropogenic sources included the industrialised highveld of South Africa and the Copperbelt of Zambia. Results showed that maximum ozone

concentrations did not occur over or even downwind of major industrialised areas. Rather, highest ozone concentrations occurred over Zimbabwe, where upwind sources include biogenic VOC and NO<sub>x</sub> sources from Mozambique and anthropogenic VOC and NO<sub>x</sub> sources. Thus, a combination of biogenic and anthropogenic sources was found to contribute to high ozone concentrations.

#### *Calculating Emission Estimates*

Otter *et al* (2003) calculated BVOC emission estimates for individual land cover types based on measurements of species-level emission rates. This method requires measurements from hundreds of species, as well as detailed land cover maps with associated species composition. Species-level emission rates were assigned based on published emission rates. Inevitably, emission rates could not be assigned to all species, in which case a taxonomic approach was used. If no species level data was available, an average emission rate was calculated for the genera and family level based on existing data of species in that genera or family. This method meant that each species had an assigned emission rate, and combined with species composition data could determine emission rates per land cover type. Emission rates were estimated for land cover types with no species composition data, for example deserts and plantations. Land cover data included a vegetation map developed by the South African National Botanical Institute (SANBI) with an associated species composition data set (Rutherford *et al*, 2000). A land use map with urban and agricultural areas was combined with the vegetation map so as to create a more realistic cover of vegetation.

The databases used by Otter *et al* (2003) have been maintained and updated and subsequently used to update global emission estimates of BVOCs (Guenther *et al*, 2006, Wiedinmyer *et al*, 2006). A global map of BVOC emission rates with a 1 km spatial resolution can be downloaded at <http://cdp.ucar.edu/>.

#### **Importance of Isoprene as a BVOC**

BVOCs include hundreds of individual compounds that are produced and emitted, in varying degrees, by plants (Seinfeld and Pandis, 1998). However, based on the emission rate measurements of individual species and landscape level measurements, BVOCs are

typically divided into four categories. The first category represents an individual compound, isoprene, which accounts for about half of all BVOCs emitted on a global scale. Guenther *et al* (1995) estimated total global BVOC emissions of 1150 Tg C yr<sup>-1</sup> of which 44 % was isoprene. Of the 80 Tg C yr<sup>-1</sup> estimated for Africa south of the equator, 70 % is isoprene (Otter *et al*, 2003). The Africa results were supported with ground measurements that showed isoprene to be the most abundant BVOC emitted from forests and savannas (Greenberg *et al*, 1999). The second category is a group of compounds called monoterpenes which include, amongst others,  $\alpha$ -pinene and  $\beta$ -pinene. Monoterpenes represent 11 % of global and 8.7 % of African south of the equator BVOC emissions (Guenther *et al*, 1995, Otter *et al*, 2003). The remaining compounds are grouped as 'other VOCs' which can be further divided into 'other reactive VOCs' and 'other VOCs'. Thus, it is evident that isoprene is the single highest emitted biogenic volatile organic compound.

#### *Temperature Dependence of Isoprene*

It is not clear what the biological role of isoprene is, or where exactly it is produced in the plant cell (Karl *et al*, 2002, Sharkey *et al*, 2007). However, it is clear that isoprene emission rates are temperature and light dependent (Sanadze, 1991, Monson *et al*, 1992, Sharkey *et al*, 1996, Harley *et al*, 1996, Harley *et al*, 1997, Singsaas and Sharkey, 2000), and that isoprene is emitted through the stomata (Harley *et al*, 1996). Isoprene production is controlled by an enzyme, isoprene synthase, (Silver and Fall, 1991) which accounts for the temperature dependence of emissions. Emissions increase exponentially up to about 40 °C, after which they decrease again (Monson *et al*, 1992, Sharkey *et al*, 1996, Harley *et al*, 1996, Harley *et al*, 1997, Singsaas and Sharkey, 2000).

Isoprene synthase is not found in all plant species, and as a result emissions are species-specific (Silver and Fall, 1991). Emissions are specific to the point that there are emitting and non-emitting species in the same genera (Sharkey *et al*, 1996). This highlights the value of measuring isoprene emission rates of individual species and then scaling up to a landscape level, as applied by Otter *et al* (2003) for Africa south of the equator. If there is a change in species composition of a landscape, new emission rate estimates can be calculated accordingly.

### *Light Dependence of Isoprene*

Field studies show that isoprene emissions increase almost linearly with light intensity and then saturate (Sharkey *et al.*, 1996, Harley *et al.*, 1996, Harley *et al.*, 1997). Evidence suggests that isoprene production requires products from photosynthesis and that this explains the observed light dependence. Early studies showed that labeled carbon used in photosynthesis appeared in isoprene produced by plants (Sanadze, 1966, Sanadze, 1991). The production pathway has since been identified (Figure 1.1) and the discovery of the active enzyme, isoprene synthase, supports the suggested pathway (Silver and Fall, 1991, Sharkey *et al.*, 1991). Isoprene is a 5-carbon compound ( $C_5H_8$ ) with two double bonds. Isoprene is mainly produced when a 2-carbon compound produced after carbon fixation, Acetyl Coenzyme A, enters the mevalonic acid cycle and is converted to a 5-carbon compound (McMurry, 2007). The 5-carbon compound, Isopentenyl Pyrophosphate (IPP), is then converted to Dimethylallyl Pyrophosphate (DMAPP) by isomerase. DMAPP is then converted to isoprene by isoprene synthase (Figure 1.1). Other pathways have been identified, for example the acidification of DMAPP, but produce negligible amounts of isoprene in comparison to isoprene synthase activity (Silver and Fall, 1991, Silver and Fall, 1995).

### **Relevance on Future Emission Estimates of Isoprene**

As isoprene emissions are driven by climate variables like temperature and light, emissions are expected to change in response to climate change. Furthermore, species distribution is expected to change as climate changes (Leliaert *et al.*, 2003), altering isoprene emissions further. Thus, future predictions of isoprene emissions are relevant as they affect atmospheric chemistry and, more specifically, ozone and  $NO_x$  concentrations.



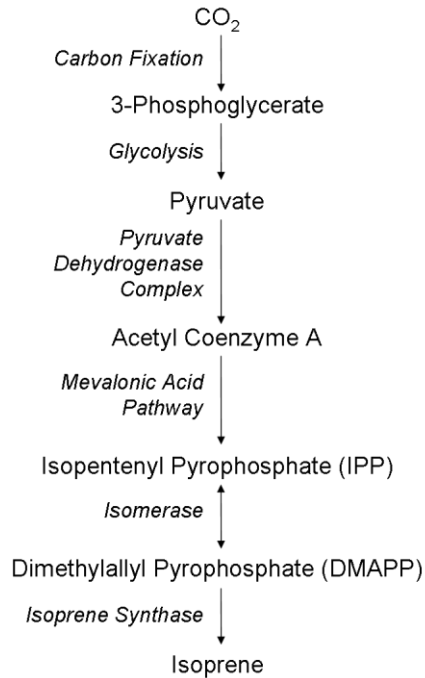


Figure 1.1: Isoprene production pathway from carbon fixation during photosynthesis (after Sharkey et al, 1991 and Lerdaun et al, 1997).

### *Land Cover Change*

The results of land cover change on biogenic emissions vary between studies. Variations can be due to the spatial scale of land cover data used. Consequently, regional and local models may include land cover changes that global models do not show (Wiedinmyer *et al*, 2006). Land cover change also depends on the vegetation model and associated database used. In some cases, emissions decrease due to a decrease in area extent of vegetation (Constable *et al*, 1999, Sanderson *et al*, 2003). Other studies modelled an increase in woody vegetation, resulting in an increase in emissions (Turner *et al*, 1991, Guenther *et al*, 1999b). Lathière *et al* (2005) found a regional increase in emissions over Europe with an increase in forest areas, but there was no increase on a global scale. Wiedinmyer *et al* (2006) found no significant change in emissions on a global scale when land cover change was included. For both these studies, landcover change was simulated on a regional scale and not on a global scale, which is why global emission were not not affected.

### *Future Temperatures*

Future temperature increases should result in an increase in isoprene emissions (Constable *et al*, 1999, Sanderson *et al*, 2003, Guenther *et al*, 1999b, Wiedinmyer *et al*, 2006). These studies modelled the response of isoprene to temperature using an algorithm developed by Guenther *et al* (1993), which show emissions to be temperature dependent. Future temperatures used in these studies are taken from general circulation models (GCMs). Model outputs are based on climate scenarios where there is a doubling of CO<sub>2</sub> concentration.

### *Changes in Radiation*

The effect of light dependence in studies estimating future isoprene emissions is generally not explained well. Guenther *et al* (1999b) use a canopy model to allow for changes in light intensity. Turner *et al* (1991) incorporate light using a photoperiod (length of day) value. Other studies are not explicit on how light is incorporated into future emissions (Constable *et al*, 1999, Sanderson *et al*, 2003, Wiedinmyer *et al*, 2006). Although these studies may indeed use light intensity values from GCM data, it is not clear. Results have rather focused on the effect of temperature and land cover change.

### *Effect of Elevated CO<sub>2</sub>*

Elevated CO<sub>2</sub> concentrations will increase atmospheric temperature and consequently isoprene emissions. However, studies show that elevated CO<sub>2</sub> will alter BVOC emissions from vegetation. Sharkey *et al* (1991) found that isoprene emissions increased in Oak leaves when CO<sub>2</sub> partial pressure was increased. However, isoprene emissions from Aspen decreased by 30 to 40 % when CO<sub>2</sub> partial pressure was increased. Monson and Fall (1989) also found that Aspen isoprene emissions decreased under elevated CO<sub>2</sub>. A study on a plantation of Eastern Cottonwood (*Populus deltoids*) under controlled conditions showed that isoprene emissions decreased by 21 % and 41 % under elevated CO<sub>2</sub> (Rosenstiel *et al*, 2003). Isoprene emissions from Northern Red Oak (*Quercus rubra*) were also found to decrease under elevated CO<sub>2</sub> emissions (Loreto and Sharkey, 1990). These studies point towards the possibility that isoprene emissions will decrease under elevated CO<sub>2</sub>. An increase in the partial pressure of CO<sub>2</sub> effects plant physiology

that produces isoprene. This has implications when choosing a doubled CO<sub>2</sub> climate scenario. Increased CO<sub>2</sub> will increase ambient temperatures which will increase emissions if the temperature algorithm is used. However, elevated CO<sub>2</sub> may also decrease isoprene emissions. The response of isoprene emissions to elevated CO<sub>2</sub> would have to be recalculated for individual species and incorporated when calculating future emission rates. Until this relationship is more rigidly incorporated into future emissions, projected emissions should be considered as over estimations (Guenther *et al*, 2006). A recent study did incorporate CO<sub>2</sub> algorithms that affect isoprene emissions (Heald *et al*, 2009). Results showed that elevated CO<sub>2</sub> can offset future isoprene emissions caused by increased temperature when landcover change is not included. However, when landcover change is included, emissions were still found to increase.

### **Estimating Future Temperatures Using a Regional Climate Model**

General circulation models (GCMs) simulate the atmosphere at regular grid points across the world using finite-difference equations (Stull, 2000). A number of vertical levels are included at each grid point in the GCMs, thus creating a three dimensional grid. Finite-difference equations are applied to each grid point and for each time step in the model run. Typically, GCMs are run over a period that is representative of the climate, usually about 30 years. To test the performance of a GCM, a control simulation is run for the current climate, normally from about 1970 to 2000, and results are then verified against observed data from that period. Once the model is deemed to have simulated the current climate adequately, the future climate can be modelled, usually over the years 2070 to 2100.

General circulation models are limited to a coarse horizontal resolution of about 1° longitude by 1° latitude. This is due to computational limitations as a result of the high number of calculations required for each grid point and time step in the GCM. Regional climate models (RCMs) are used to downscale GCMs and derive atmospheric features that occur at scales smaller than 1° (Engelbrecht, 2005). Different methods can be applied when using RCMs to downscale GCMs. The first is empirical, or statistical, downscaling and the second is dynamical downscaling. Both methods of downscaling make use of a grid that has a higher resolution than a GCM, usually about 0.5°, and extends over a

region of interest. Thus, simulations of the atmosphere are determined at higher resolutions than that represented in the GCM.

*Predicting Future Scenarios of Temperature Increase using General Circulation Models*

Predictions of future emissions of greenhouse gases are presented by the Intergovernmental Panel on Climate Change (IPCC) in a Special Report on Emissions Scenarios (SRES). Temperatures are expected to increase as concentrations in greenhouse gases increase. To determine the extent to which temperature will increase, GCMs make use of future emission scenarios of greenhouse gases. These scenarios take into consideration the driving forces of greenhouse gas emissions like population growth, demand for energy and advances in technology (IPCC SRES, 2000). As these scenarios are fed into GCMs and represent a range of possible future conditions, the output from the GCMs represents a range of possible future increases in temperature. The following greenhouse gases are used in the SRES; anthropogenic emissions of carbon dioxide (CO<sub>2</sub>), methane (CH<sub>4</sub>), nitrous oxide (N<sub>2</sub>O), hydrofluorocarbons (HFCs), perfluorocarbons (PFCs), sulfur hexafluoride (SF<sub>6</sub>), hydrochlorofluorocarbons (HCFCs), chlorofluorocarbons (CFCs), the aerosol precursor and the chemically active gases sulfur dioxide (SO<sub>2</sub>), carbon monoxide (CO), nitrogen oxides (NO<sub>x</sub>), and non-methane volatile organic compounds (NMVOCs) (IPCC SRES, 2000). The emission scenarios are divided into four categories or families, namely A1, A2, B1 and B2. The A1 family assumes global co-operation in implementing new technologies, thereby decreasing regional differences in per capita greenhouse gas emissions. The A1 family is further divided into three scenarios based on sources of energy usage. The first scenario is fossil fuel intensive; the second is an alternative or non-fossil fuel approach and the third is a balance between scenarios one and two. The A2 family is in contrast to the A1 family; Economic development and implementation of new technologies is expected to be more fragmented, thereby highlighting differences between regions. Furthermore, implementation of new technologies is assumed to be slower than in the A1 family. Additionally, population growth is expected to be higher than in scenario A1, resulting in a higher global population. Family B1, like family A1, assumes global co-operation in implementing new technologies and the same population growth rate. Economic growth

is assumed as in A1, but in different sectors like service and information that are less reliant on natural resources. Family B2 is similar to family A2 in that it predicts less cohesive implementation of new technologies. Like A2, economic progress is localised to regions; however, population growth is not expected to be as high as in A2. None of these families is a preferred scenario but rather have the same probability of occurring (IPCC SRES, 2000). They simply serve as a range of possibilities of what may occur in the future, thus allowing for a range of uncertainty when predicting future greenhouse gas emissions and the associated effects on climate.

#### *The Conformal-Cubic Atmospheric Model*

The Conformal-Cubic Atmospheric Model (C-CAM) is a regional climate model that applies dynamical downscaling of GCM simulations (Engelbrecht, 2005). C-CAM makes use of variable resolution global modelling when creating the grid for the area of interest. In this method, a high resolution grid is applied to the area of interest, after which the resolution increases with distance from the area of interest. This is in contrast to limited area models, which use a high resolution grid for the area of interest only. Engelbrecht (2005) used C-CAM to dynamically downscale output from the Commonwealth Scientific and Industrial Research Organisation (CSIRO) Mk3 Ocean-Atmosphere General Circulation Model (OAGCM) for Africa south of the equator for the present day climate and a future climate. The current climate extended over a thirty-year period from 1975 to 2005 while the future period extended from 2070 to 2100. A grid resolution of  $0.5^\circ$  was used and future climate simulations were based on SRES A2 scenario. C-CAM simulations of temperature for the current climate corresponded well to observed temperatures from the Climate Research Unit (CRU) dataset (Engelbrecht, 2005). Based on the definitions of the SRES scenarios, future temperatures based on SRES A2 can be considered as a worst case scenario.

#### **Estimating Emissions using an Emissions Model**

Emission models are used to calculate BVOC emission rates in response to driving variables like temperature and light. Guenther *et al* (1993) developed algorithms representing isoprene emission response to temperature and light based on observed

measurements that were made in field and laboratory studies. These algorithms have been compared to actual emission data and have been found to represent emissions well (Geron *et al*, 2000). Consequently, many studies have modelled emissions using these algorithms (Guenther *et al*, 1995, Constable *et al*, 1999, Guenther *et al*, 1999b, Otter *et al*, 2003, Sanderson *et al*, 2003, Wiedinmyer *et al*, 2006). Modifications to the algorithms have been made periodically, where the latest version is included in the global emissions model, Model of Emissions of Gases and Aerosols from Nature (MEGAN v2.04) version 2.04 (Guenther *et al*, 1995, Guenther *et al*, 1999a, Guenther *et al*, 2006).

The MEGAN model algorithms are applied to each grid point of a user defined grid. The user defines the size of the domain for the area of interest and the horizontal resolution of the grid. Regular grid spacing is used and resolutions range from 1km to 0.5° (~60km) in practice. As MEGAN is a global model, the user can define a global grid and apply a suitable projection. However, the model algorithms are solved for each grid cell and the final emission rate is calculated independent of any conditions in adjacent cells. Consequently, as there are no interactions between adjacent grid points, a limited area grid can be defined without causing any deficiency in model performance. Typically, a single vertical layer representing the surface level is used.

An overview of model inputs will be discussed here. Algorithms will be discussed in more detail as part of the methodology chapter.

### *Model Inputs*

Emission models generally take the form:

$$E = \varepsilon \cdot \gamma_T \cdot \gamma_{PPFD} \cdot \gamma_{LAI}$$

Where: E = Output emission rate (gC m<sup>-2</sup> s<sup>-1</sup>)

ε = emission factor (gC m<sup>-2</sup> s<sup>-1</sup>)

γ = emission activity in response to temperature (T), light (PPFD is photosynthetic photon flux density) and leaf area index (LAI) (no units)

### *Emission factor*

In general, an emission factor is an emission rate under standard conditions. In terms of BVOCs, the emission factor is the emission rate from a species or land cover type that

typically has been standardized to a temperature of 30 °C and light intensity of 1000  $\mu\text{mol m}^{-2} \text{s}^{-1}$ . This standardisation effectively allows for the comparison of source strengths of isoprene emissions between species and land cover types.

### *Emission Activities*

The emission activities are the response of isoprene emissions to driving variables like temperature and light. These are represented by algorithms and show how emissions vary relative to standard conditions. For example, assume an emission factor of 100  $\text{gC m}^{-2} \text{s}^{-1}$  at 30 °C and 1000  $\mu\text{mol m}^{-2} \text{s}^{-1}$ . The emission activity under standard conditions is 1, so the emission rate will be 100  $\text{gC m}^{-2} \text{s}^{-1}$ . However, if temperature increased to 35 °C, the emission activity for temperature will increase, for example, to 1.2. The new emission rate (E) is now 120  $\text{gC m}^{-2} \text{s}^{-1}$ , but the emission factor is still 100  $\text{gC m}^{-2} \text{s}^{-1}$ .

### *Leaf Area Index*

As isoprene is emitted from the stomata on the leaves, a source density value, representing the area of leaf present, needs to be included in the emission model. This is normally represented as a leaf area index (LAI), which is  $\text{m}^2$  of leaf per  $\text{m}^2$  of ground. If the study domain is small enough, LAI values can be measured in the field (Klinger *et al*, 1998). Alternatively, LAI over larger areas can be retrieved from MODIS images provided that scenes are not affected by cloud cover (Guenther *et al*, 1995 and Otter *et al*, 2003). Emission activity, and therefore emission rates, saturate at high LAI values, as shading decreases the light intensity (Figure 1.2). Emission activities for temperature and light will be discussed in the next section.

### **Emission Activity and Model Uncertainty**

Temperature causes the greatest variation in isoprene emission activity (Figure 1.2). From Figure 1.2 we can see that the emission activity in response to temperature and leaf area index (LAI) contains steep gradients which result in the greatest changes in emission activity. However, the range of LAI values that fill these conditions (steep gradient) is small compared to temperature, where -100 to -60 % equals LAI of 0 to 2  $\text{m}^2\text{m}^{-2}$ , but -40 to 20 % equals 18 to 36 °C. Additionally, temperature accounts for the greatest increase in emission activity of 60 % when increased by 20 % from standard conditions. The

response of emissions to light (Pac) is almost linear and will eventually saturate. The next section will focus on the effect of temperature on emission activity and the combined effect with other physical conditions.

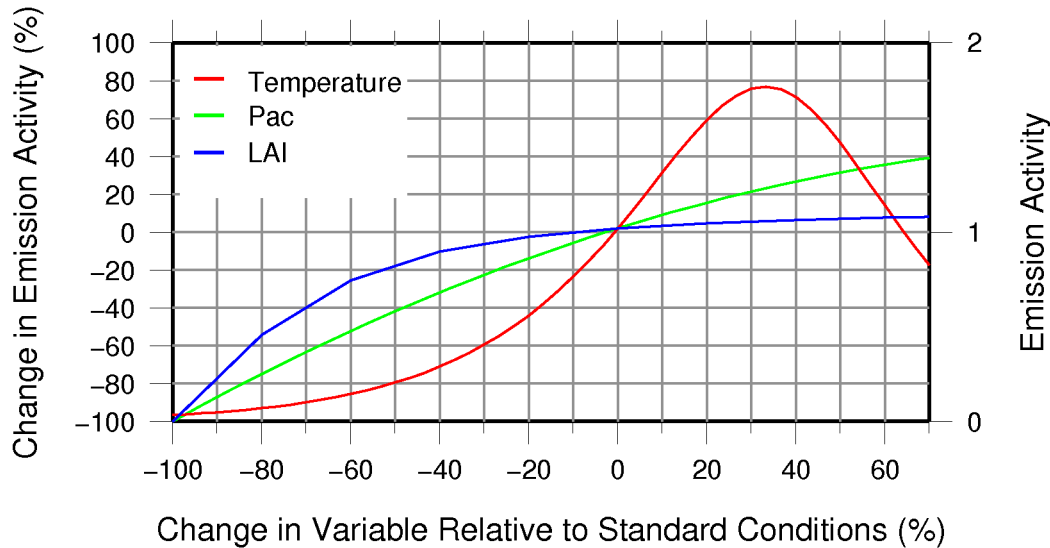


Figure 1.2: Change in emission activity in response to change in model inputs (after Guenther *et al*, 2006): temperature, Pac (above canopy photosynthetically active radiation) and LAI (leaf area index). For each line, two inputs are kept constant while the third changes (e.g. red line = change in temperature). ‘0’ on the x-axis represents standard conditions (Temperature = 30 °C, ppfd transmission = 0.6, LAI = 5m<sup>2</sup>m<sup>-2</sup>). ‘0’ on the y-axis represents an emission activity of 1.

### *Temperature produces the most uncertainty*

It was established in the previous section that, of the input variables currently included in MEGAN, temperature produces the greatest range of variation of model output. The question now is: how much will other physical conditions amplify the change in emission activity? An increase in above-canopy light intensity (Pac), daily average Pac (dppfd) or daily average temperature (average temperature over past 24 hours) will cause an increase in emission activity (Guenther *et al*, 2006). These three cases will be considered in this section.

An increase in Pac increases the amplitude of emission activity with the greatest change occurring at higher temperatures, ranging from about 35 to 40 °C (Figure 1.3). An



increase in dppfd increases emission activity over the same temperature range as Pac (Figure 1.4). However, the range of change in emission activity is not as wide with dppfd as it is with Pac at high temperatures (100% from 40% to 140 % and 190% from -85% to 105 % respectively). An increase in daily average temperature shows a different pattern. There is a larger range in emission activity and maximum emission activity occurs at increasingly higher temperatures (Figure 1.5). This pattern shows the dependence of temperature and average temperature on each other, assuming that the higher the temperature, the higher the average temperature will be.

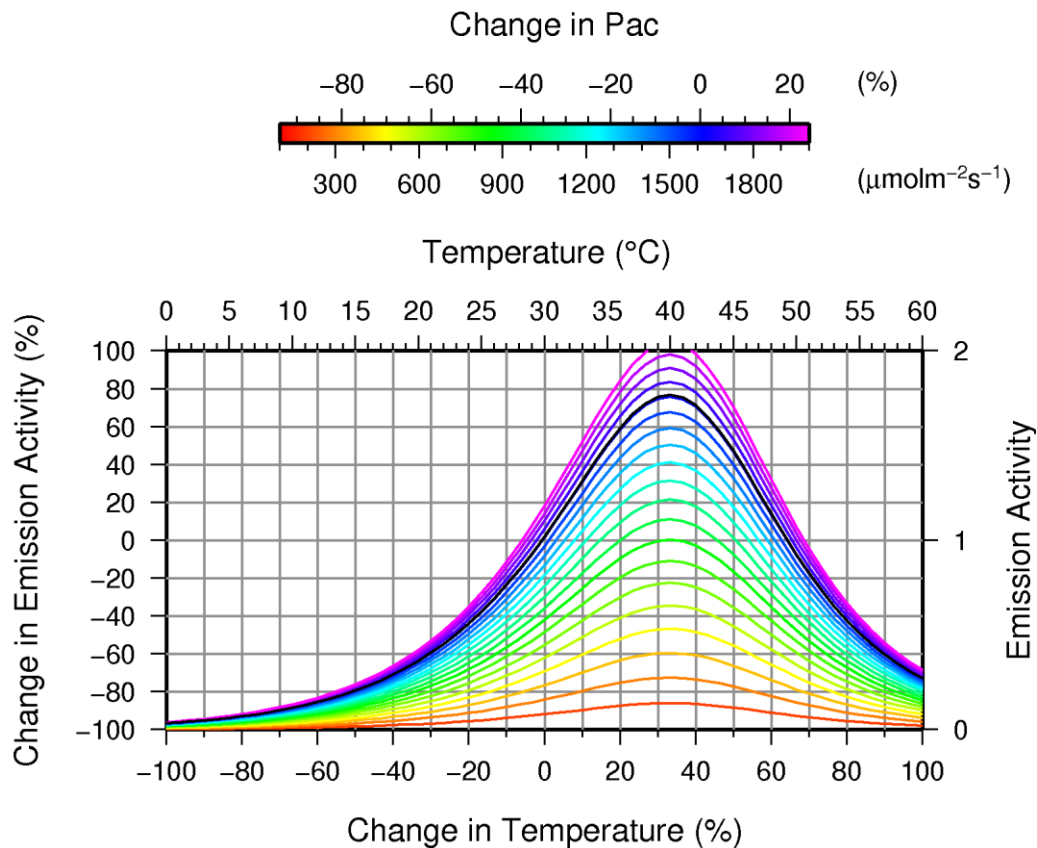


Figure 1.3: Pac is above canopy photosynthetically active radiation. The black line represents standard conditions. Under standard conditions Pac is  $1610.2 \mu\text{mol m}^{-2}\text{s}^{-1}$  while solar angle is  $60^\circ$ , resulting in photosynthetic photon flux density (ppfd) transmission of 0.6, as used by Guenther *et al* (2006).

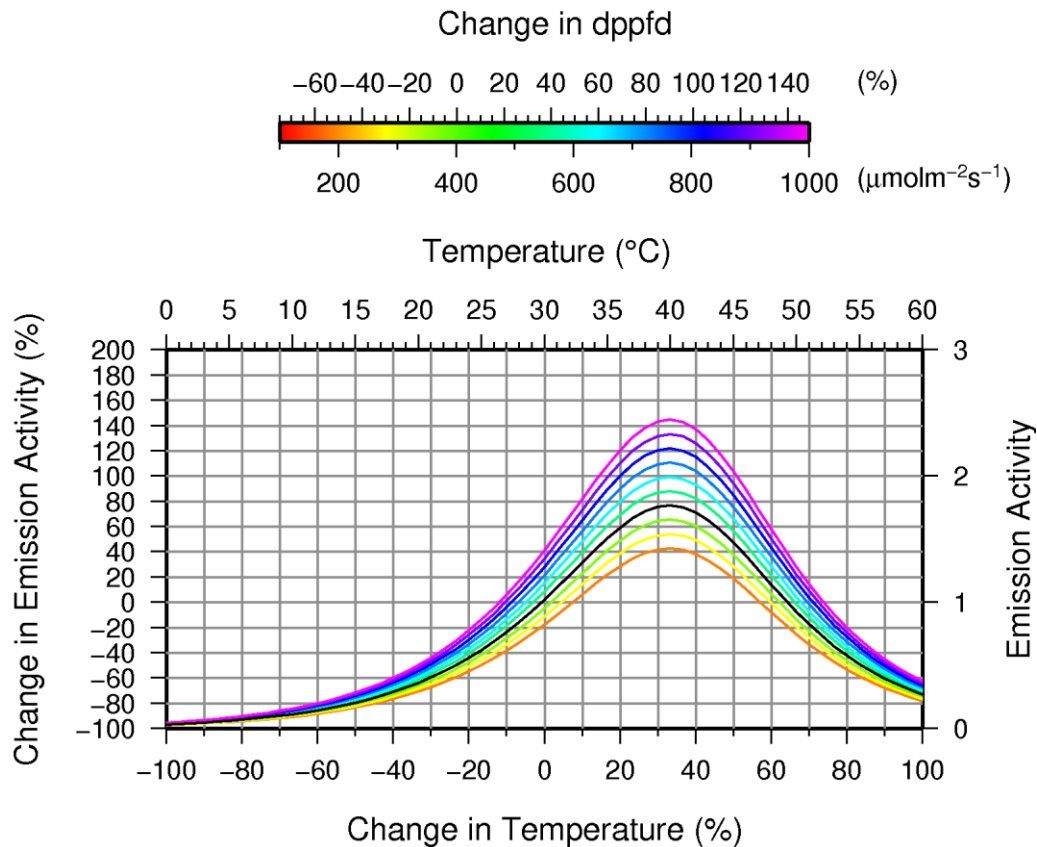


Figure 1.4: dppfd is average photosynthetically active radiation for the past 24 hours. The black line represents standard conditions. dppfd is  $400 \mu\text{mol m}^{-2}\text{s}^{-1}$  under standard conditions. This results in a photosynthetic photon flux density (ppfd) transmission of 0.6, as used by Guenther *et al* (2006).

A more meaningful way of comparing model inputs and output is to use the same percentage change in input. In other words, how much does a 20 % increase in an input change emission activity? A summary of comparisons can be found in Table 1.2. An increase of 20 % corresponds to values of Pac, dppfd and daily average temperature of about  $1950 \mu\text{mol m}^{-2}\text{s}^{-1}$ ,  $490 \mu\text{mol m}^{-2}\text{s}^{-1}$  and  $29 \text{ }^\circ\text{C}$  respectively (Table 1.2). All variables caused an increase in emission activity, but average temperature caused the greatest increase. From these results it is clear that emission activity is affected most by temperature and daily average temperature.

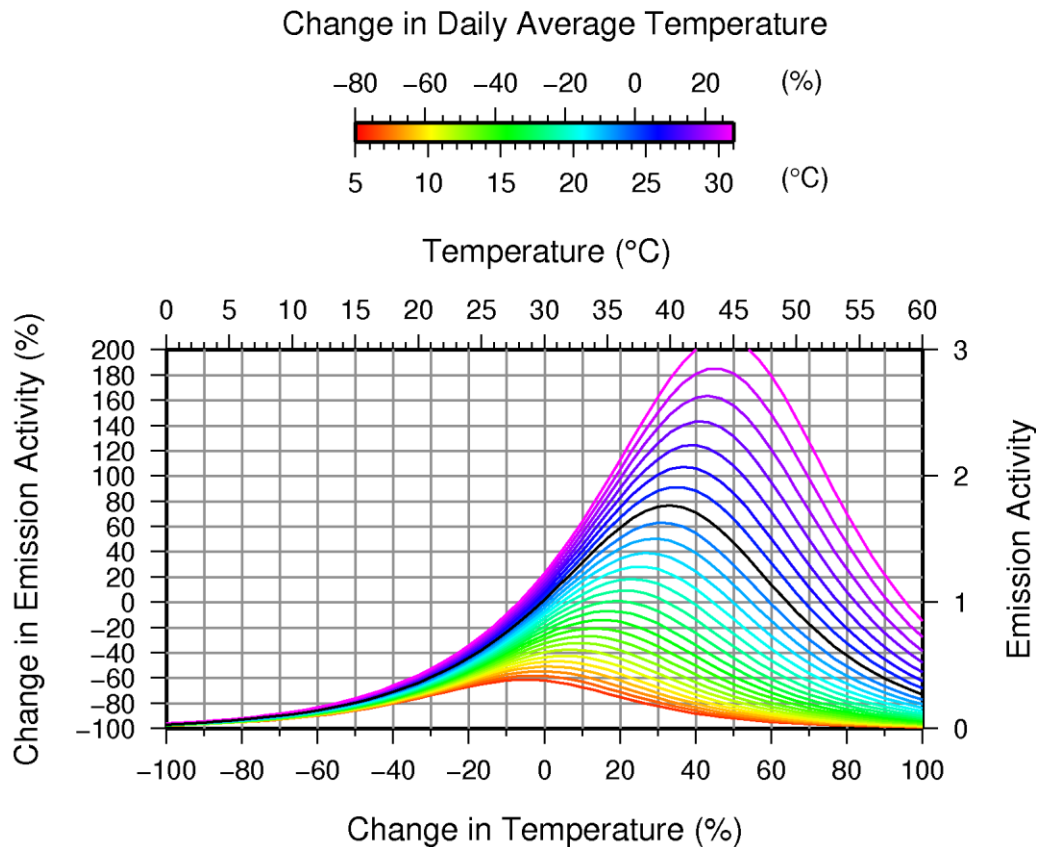


Figure 1.5: Daily average temperature is the temperature for the past 24 hours. The black line represents standard conditions. Daily average temperature is 24 °C under standard conditions (after Guenther *et al*, 2006).

Table 1.2: Change in emission activity for a 20 % increase from standard conditions of Pac, dppfd and daily average temperature. An increase of 0 to 6 °C in standard temperature equals a 20% increase in temperature. Similarly, 0 to 9 °C represents a 30% increase.

Input	Increase in input (units)	Increase in Input (%)	Increase in Emission Activity	Range of Increase	Net Increase
Temp	0 to 6 °C	0 to 20 %	0 to 60 %	60 %	0 % (Base Case)
Pac	0 to 339.8 $\mu\text{mol m}^{-2}\text{s}^{-1}$	0 to 20 %	~ 17 to 80 %	~ 60 %	~ 20 %
Dppfd	0 to 90 $\mu\text{mol m}^{-2}\text{s}^{-1}$	0 to 20 %	~ 5 to 65 %	~ 60 %	~ 5 %
Avg T	0 to 5 °C	0 to 20 %	~ 20 to 100 %	~ 80 %	~ 40 %
Temp	0 to 9 °C	0 to 30 %	0 to 75 %	75 %	0 % (Base Case)
Pac	0 to 339.8 $\mu\text{mol m}^{-2}\text{s}^{-1}$	0 to 20 %	~ 17 to 100 %	~ 80 %	~ 25 %
Dppfd	0 to 90 $\mu\text{mol m}^{-2}\text{s}^{-1}$	0 to 20 %	~ 5 to 80 %	~ 75 %	~ 5 %
Avg T	0 to 5 °C	0 to 20 %	~ 20 to 140 %	~ 120 %	~ 65 %

## Summary and Objectives

The role of isoprene in atmospheric chemistry has been highlighted in this chapter. The use of an emissions model in calculating isoprene emissions has been discussed, noting some advantages when calculating emissions at a regional scale. Furthermore, an argument for the importance of estimating future isoprene emissions has been made.

In this study, the MEGAN emissions model will be run for southern Africa to determine isoprene emission rates for the current climate and a future climate. Isoprene was chosen because it is the single highest emitted BVOC from vegetation. Furthermore, this saves computational and software error fixing time. Climate data will be acquired from the dynamically downscaled regional climate model (RCM), Conformal-Cubic Atmospheric Model (C-CAM). This study will be the first regional study over southern Africa to use MEGAN and dynamically downscaled RCM output.

Objectives include:

- Identifying areas with high isoprene emissions.
- Identifying the driving variable/s of isoprene emissions over these areas.
- Verifying that emissions are sensitive to temperature as expected.
- Identifying areas that are most affected by temperature sensitivity.

## CHAPTER 2: DATA AND METHODOLOGY

This chapter follows the following structure: Firstly, a description of the model is given, highlighting parameters and algorithms relevant to this study. Secondly, the process of running the model is followed systematically. Relevant input data will be discussed as and when it enters the process. This section also includes descriptions of any alterations made to the MEGAN model code. Thirdly, calculations used in processing model output are presented as well as a description of identifying driving variables of isoprene emissions. Finally, a description of the sensitivity analysis to temperature is given.

### Overview of MEGAN

MEGAN accounts for the driving forces of isoprene emission rates through the use of algorithms which were initially developed by Guenther *et al* (1993) and later updated to their current form in MEGAN (Guenther *et al*, 2006). Algorithms represent emission response to the main driving forces of temperature, light and leaf area index. When these algorithms are combined with an emission factor for isoprene, the emission rate can be calculated (equation (2.1) and (2.2)).

Although MEGAN is a global model, the user can define a smaller modelling domain that is more specific to a region of interest. The user defines a grid of regular points, specifying the horizontal resolution which is applied in the x (longitude) and y (latitude) direction. The horizontal resolution typically varies from 0.5° to 1km depending on the size of the model domain. Typically, only one vertical level representing surface emission rates is used. Input variables are required for each grid cell in the model and domain and MEGAN then applies equations (2.1) and (2.2) to each point. The final consideration is the temporal resolution of the model. In this study, hourly temperature and light data was applied for the months of January and July. The final output is an emission rate for isoprene for each grid cell and each hour, which is later converted into a total monthly emission rate.

BVOC emission models like MEGAN and its predecessors have mostly been used in quantifying BVOC emissions either globally or regionally (Guenther *et al*, 1995, Guenther *et al*, 2000, Otter *et al*, 2003, Wiedinmyer *et al*, 2001, Wiedinmyer *et al*, 2005). More recently, temperature data from general circulation models has been used as emission model input, which has naturally lead to estimating future BVOC emission based on future temperature scenarios (Guenther *et al*, 2006, Wiedinmyer *et al*, 2006). This dissertation presents BVOC emission model results for southern Africa for the current climate and a future climate using a dynamically downscaled regional climate model. The model domain extends from 10° to 36° east and 16° to 36° south (Figure 2.1).

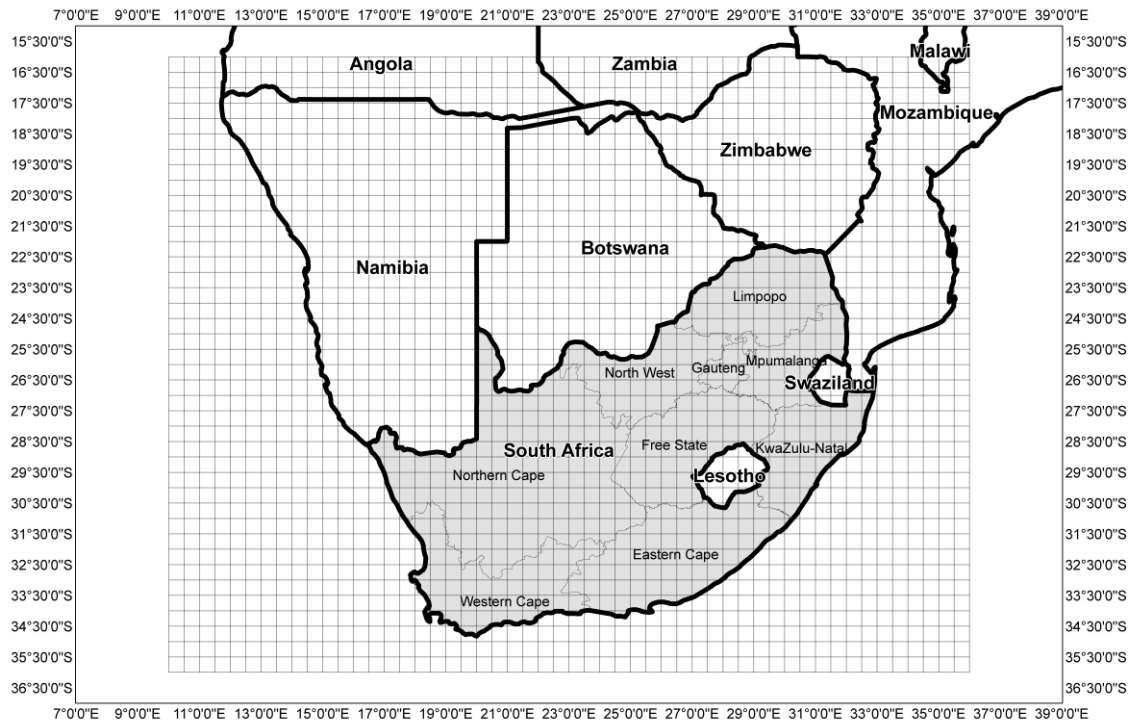


Figure 2.1: Model domain with half degree model grid. Domain extends from 10° to 36° east and 16° to 36° south.

### MEGAN Algorithms

Isoprene emission rates were modelled using MEGAN v2.04 (Guenther *et al*, 2006). Guenther *et al* (2006) contains a full description of all model equations and algorithms. Algorithms relevant to this study are given below. Emission rate estimates are calculated for each grid cell as grams of Isoprene per second ( $gs^{-1}$ ) using equation (2.1).

$$\text{Emission rate} = \varepsilon \cdot \gamma \cdot \rho \quad (2.1)$$

Where:

- $\varepsilon$  = Emission factor ( $\mu \text{ gm}^{-2} \text{ s}^{-1}$ )
- $\gamma$  = Emission activity in response to the physical environment
- $\rho$  = Canopy production and loss of isoprene

The use of a detailed canopy model is optional when running the emissions model, and was not used in this study. Consequently, the value for canopy production and loss ( $\rho$ ) was set to 1 and does not affect emission estimates. Furthermore, physical conditions in the vegetation canopy that control emissions are included in the canopy environment emission activity ( $\gamma_{\text{CE}}$ ) (Equation (2.2)). There are two sets of algorithms available to calculate  $\gamma_{\text{CE}}$ , depending on the canopy model used. The algorithms that do not require a detailed canopy model are described below and are used in calculating emission estimates.

$$\gamma = \gamma_{\text{CE}} \cdot \gamma_{\text{AGE}} \cdot \gamma_{\text{SM}} \quad (2.2)$$

Where:

- $\gamma_{\text{CE}}$  = Canopy Environment Emission Activity  
=  $\gamma_{\text{T}} \gamma_{\text{PPFD}} \gamma_{\text{LAI}}$
- $\gamma_{\text{T}}$  = Emission response to temperature
- $\gamma_{\text{PPFD}}$  = Emission response to photosynthetic photon flux density (ie. Light)
- $\gamma_{\text{LAI}}$  = Emission response to leaf area index
- $\gamma_{\text{AGE}}$  = Leaf age emission activity
- $\gamma_{\text{SM}}$  = Soil Moisture emission activity

Emission activity values for leaf age and soil moisture were set to a default value of 1 and therefore do not affect emission estimates. Emission activities in response to temperature, PPFD and leaf area index (LAI) were calculated and are given in equations (2.3), (2.4) and (2.5).

$$\gamma_{\tau} = \frac{E_{opt} \cdot CT2 \cdot \exp(CT1 \cdot x)}{[CT2 - CT1 \cdot (1 - \exp(CT2 \cdot x))]} \quad (2.3)$$

Where:

$$\begin{aligned} x &= [(1/T_{opt}) - (1/Thr)] / 0.00831 \\ E_{opt} &= 1.75 \cdot \exp(0.08 \cdot (T_{daily} - 297)) \\ CT1 &= 80 \\ CT2 &= 200 \\ Thr &= \text{hourly average air temperature (K)} \\ T_{daily} &= \text{daily average air temperature (K)} \\ T_{opt} &= 313 + 0.6 \cdot (T_{daily} - 297) \end{aligned}$$

$$\gamma_{PPFD} = \sin(a) [ 2.46 \cdot (1 + 0.0005 \cdot (P_{daily} - 400)) \cdot \phi - 0.9 \cdot \phi^2 ] \quad (2.4)$$

Where:

$$\begin{aligned} a &= \text{solar angle (degree)} \\ P_{daily} &= \text{daily average above canopy PPFD } (\mu \text{ mol m}^{-2} \text{ s}^{-1}) \\ \phi &= \text{above canopy PPFD transmission (no dimension)} \\ &= \frac{P_{ac}}{\sin(a) \cdot P_{toa}} \end{aligned}$$

Where:

$$\begin{aligned} P_{ac} &= \text{above canopy PPFD } (\mu \text{ mol m}^{-2} \text{ s}^{-1}) \\ P_{toa} &= 3000 + 99 \cdot \cos[2 \cdot 3.14 \cdot (DOY - 10)/365] \\ DOY &= \text{Day of year} \end{aligned}$$

The algorithm representing the emission activity to light (equation (2.4)) is only valid when the sun is above the horizon, in other words when the solar angle is greater than 0 and less than 180 degrees. If the solar angle is below the horizon, in other words less than or equal to 0 or greater than or equal to 180 degrees, then  $\gamma_{PPFD}$  is 0.

$$\gamma_{LAI} = \frac{0.49 \cdot LAI}{(1 + 0.2 \cdot LAI^2)^{0.5}} \quad (2.5)$$



Where:

LAI = leaf area index ( $m^2 m^{-2}$ )

## A Brief Explanation on Interpreting Model Outputs

### *Contribution of Model Inputs in Calculating Model Output*

A summary of the model equations as they are used in this study is shown in equation (2.7). Emission rates were normalized for leaf age, soil moisture and canopy production and loss. Values for these parameters were equal to 1. This means that emission rates are sensitive to the emission factor ( $\varepsilon$ ) and the emission activity for temperature ( $\gamma_{\text{Temperature}}$ ), light ( $\gamma_{\text{PPFD}}$ ) and LAI. The emission activity ( $\gamma$ ) represents how emissions respond to the physical environment. For example, if the emission activity ( $\gamma$ ) in equation 1 is 0.8 and canopy production and loss ( $\rho$ ) is 1, the output emission rate would be 80 % of the emission factor ( $\varepsilon$ ) due to the emission activity. Therefore, the magnitude of the emission activity for each physical parameter needs to be considered when assessing the validity of emission estimates.

$$\text{Emission rate} = \varepsilon \cdot \gamma_{\text{Temperature}} \cdot \gamma_{\text{PPFD}} \cdot \gamma_{\text{LAI}} \cdot \gamma_{\text{AGE}} \cdot \gamma_{\text{SM}} \cdot \rho \quad (2.6)$$

$$= \varepsilon \cdot \gamma_{\text{Temperature}} \cdot \gamma_{\text{PPFD}} \cdot \gamma_{\text{LAI}} \cdot 1 \cdot 1 \cdot 1$$

$$= \varepsilon \cdot \gamma_{\text{Temperature}} \cdot \gamma_{\text{PPFD}} \cdot \gamma_{\text{LAI}} \quad (2.7)$$

### *Identifying Driving Variables of Isoprene Emissions*

Each variable represented in equation (2.7) needs to be mapped in order to identify the driving variables of isoprene emission rates. This way, input data can be compared to areas that demonstrate high emission rates. Using this process, underlying driving variables will be identified for different areas within the study domain and will assist in understanding the spatial distribution of emission estimates.

## **Installing the MEGAN Software**

MEGAN v2.04 was compiled with gfortran on a Linux operating system (Ubuntu v8.04). Input files for MEGAN need to follow specific network Common Data Form (netcdf) conventions. In this case, the convention used is the Input/Output Applications Programming Interface (ioapi) or ioapi-netcdf files. This convention needs to be followed exactly, assigning the correct data types and number of characters for text strings, in order for the files to be read correctly. Output files have the same format. Software libraries required for ioapi v3 ([www.baronams.com](http://www.baronams.com)) and netcdf v3.6.2 ([www.unidata.ucar.edu/software/netcdf/](http://www.unidata.ucar.edu/software/netcdf/)) were downloaded and compiled with gfortran. NetCDF files are self-describing. This means that there is a header section at the start of the file that describes all the data, followed by the data. The header has three sections: dimensions, variables and global attributes. All other required attributes are prescribed by the naming convention of the netcdf file, which is ioapi in this case. Thus, dimensions include size of arrays and number of time steps in the data. Variable attributes include variable names, units and a short description of the variable. Global attributes are true for all variables and include descriptions of the geographic extent, projection and time stamp of the data. Open source software from Climate Data Operators ([www.mpimet.mpg.de/fileadmin/software/cdo/](http://www.mpimet.mpg.de/fileadmin/software/cdo/)), Netcdf Operators (<http://nco.sourceforge.net/>) and nctools was instrumental in handling this file type.

## **Running MEGAN**

There are three steps to running MEGAN: mg2ioapi, megan and mg2mech (Figure 2.2). Each step is initiated with a shell script that calls the relevant Fortran code. The first step, mg2ioapi, converts relevant land cover data, namely standard emission rates and leaf area index data, from a comma separated value (csv) file to an ioapi netcdf file. The second step, megan, calculates isoprene emission rates in grams of isoprene per second ( $\text{gs}^{-1}$ ) based on input meteorological data and land cover data. This second step, megan, is the main module of the model and is of most interest in this study. The third step converts the emission rates of relevant compounds to chemical mechanism species, but was not used in this study. After much data preprocessing, MEGAN can mostly be run by

manipulating the shell scripts. However, there were times when the FORTRAN code needed to be altered as will be discussed later with the relevant data.

### *Input Land Cover Data*

#### *Defining the MEGAN Model Domain*

The spatial resolution was half a degree and extended from 10° E to 36° E and 16° S to 36° S. This is the extent for which temperature data was available and covers the whole of South Africa and parts of Namibia, Botswana, Zimbabwe and Mozambique. The geographic grid of the land cover data is defined in a file called GRIDDESC. The latitude-longitude reference system was used with a cell size of about 60km (half a degree) resulting in a grid of 2080 cells (52 columns and 40 rows). Co-ordinate data for each cell is included in the csv file (Table 2.1) for the emission factor and LAI variables. Both EF and LAI data were downloaded from the UCAR community data portal (<http://cdp.ucar.edu/>) and will be described in the next paragraphs.

A finer horizontal resolution of 1km was originally intended for this study. However, due to practical constraints, a half degree resolution was settled on. Practical constraints included managing files sizes of netcdf files which were limited to 2 GB on a windows operating system. This was later solved by using a linux operating system. However, further error checking of the emissions model was required which required repeated model runs and post processing. This is very time consuming and large files sizes hindered the process.

#### *Isoprene Emission Factor Input Data*

Global isoprene emission factors with a 30 minute spatial resolution are available for download as netcdf (<http://cdp.ucar.edu/>). An average emission factor for each 30 minute grid cell is derived from 30 second emission factor data. Emission factors in this data set are based on field measurements from about 90 locations around the world (Guenther *et al*, 2006). Data relevant to the study area was extracted from the netcdf file, converted to text and inserted into the csv file.

Table 2.1: Required input for the csv file. CELL\_ID is an individual ID for a cell. X and Y are row and column index values. LAI1 is for January and LAI6 is for June LAI. Isoprene emission factor and LAI data are zero here because they are over the ocean.

CELL_ID	X	Y	LAT	LONG	ISOP	LAI1	LAI6	LAI7	LAI12
1	1	40	-16.46	10.71	0	0	0	0	0
2	2	40	-16.46	11.21	0	0	0	0	0
-	-	-	-	-	-	-	-	-	-
2079	51	1	-35.75	35.45	0	0	0	0	0
2080	52	1	-35.75	35.94	0	0	0	0	0

#### *Leaf Area Index (LAI) Input Data*

Global LAI data with a 30 minute spatial resolution is available for download as netcdf (<http://cdp.ucar.edu/>). The 30 minute LAI data is derived by Guenther *et al*, (2006) using 30 second MODIS LAI data (Zhang *et al*, 2004) and vegetation cover fraction (Hansen *et al*, 2003). Average LAI is calculated for a 30 minute cell and divided by the fraction of vegetation present in that cell (Guenther *et al*, 2006). The MODIS LAI data represents LAI during the year 2003. MEGAN requires LAI values for the current month and previous month. LAI for December, January, June and July were extracted from the netcdf, converted to text and inserted into the csv file (Table 2.1).

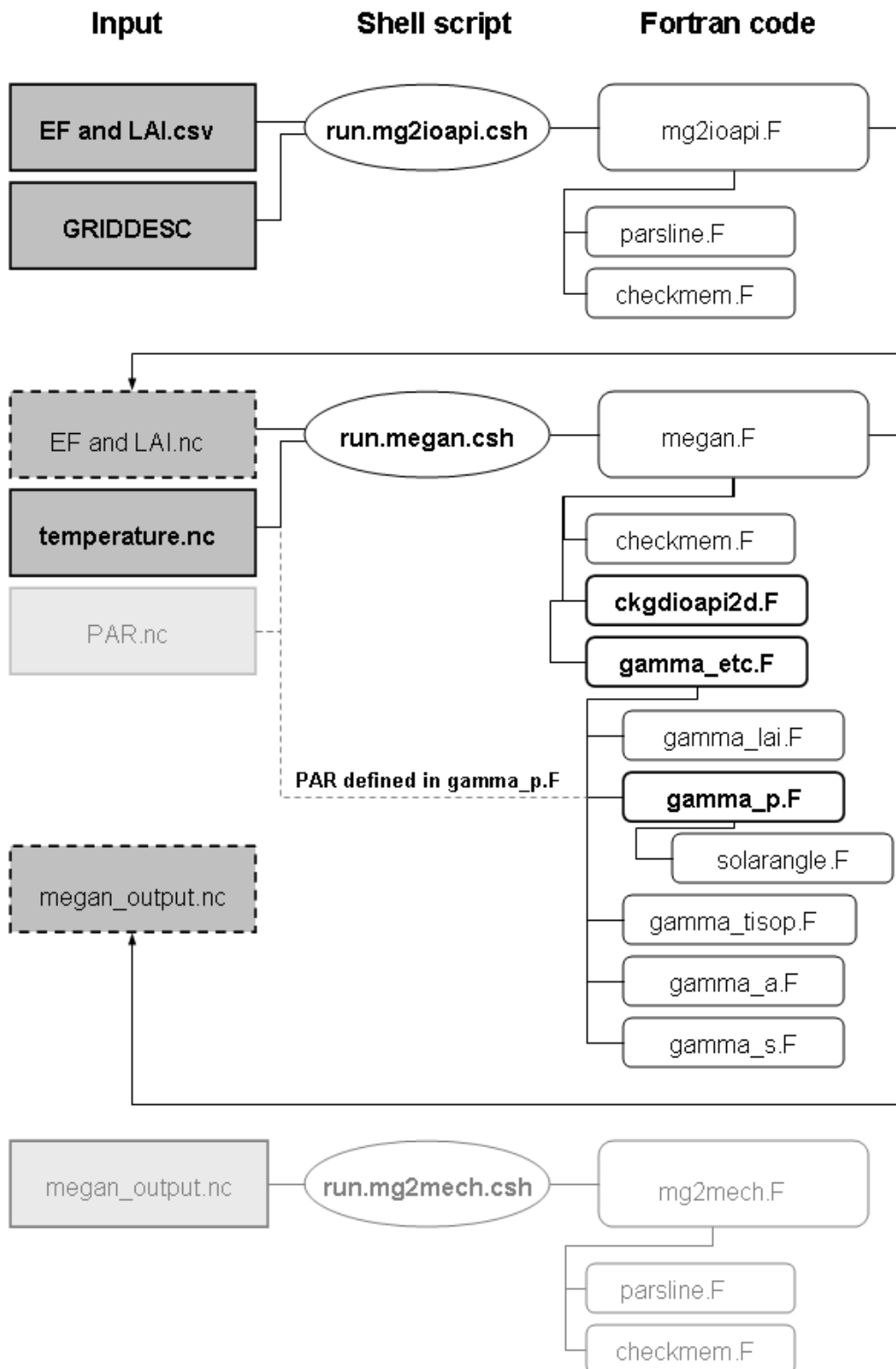


Figure 2.2: Flow diagram of MEGAN. Bold text indicates files or programs that required editing before running MEGAN. Dashed boxes indicate output files. Light grey boxes are optional and were not used in this study.

## *Calculating Isoprene Emission Rates*

### *Input Temperature Data*

#### *Simulated Periods from the Regional Climate Model*

Emission rates were calculated for January and July using temperature data for the current climate and a projected climate. Daily minimum and maximum temperatures were obtained from the Conformal-Cubic Atmospheric Model (C-CAM). C-CAM is a dynamically downscaled regional climate model that has been used to simulate climate over southern Africa (Engelbrecht, 2005). Daily screen height temperatures are simulated over a thirty year period from 1975 to 2005 for the current climate and 2070 to 2100 for a future climate. The lower boundary forcing for C-CAM is obtained from CSIRO Mk3 OAGCM and future temperatures are based on the SRES A2 scenario (Engelbrecht, 2005). C-CAM simulations for the current climate correspond well to observed temperatures from the Climate Research Unit (CRU) dataset (Engelbrecht, 2005). Although MEGAN was run for January and July, MEGAN requires temperatures from preceding months December and June. The temperature algorithm calculates average temperature for the preceding 10 days. Thus, C-CAM data and all further temperature analysis are for December, January, June and July.

#### *Calculating Monthly Temperatures from Multi-Year Simulations*

Average maximum and minimum temperatures for each day were calculated for each thirty year period. For example, maximum temperatures for each 1 January from 1975-2005 were used to calculate an average maximum temperature for 1 January. Minimum temperatures were calculated similarly. Thus, average minimum and maximum temperatures were calculated from a thirty year period for each day in January.

### *Deriving Hourly Temperatures from Daily Minimum and Maximum Temperatures*

Hourly temperature data is required as input for MEGAN. However, C-CAM output is a minimum and maximum temperature for each day. Hourly values can be modelled by fitting C-CAM output to a sine wave, which represents a heating curve. The equation in Figure 2.3 is a good model for the sine wave with minimum temperature at 3am and maximum temperature at 3pm when plotted over the period -120 to 225 degrees. Three pm is a realistic time for maximum temperature to occur over South Africa. Hourly temperatures were calculated for each day using the equation in Figure 2.3. Hourly data was converted from text to netcdf using nctools software.

### *Input Light Data*

Isoprene emissions are dependent on photosynthetically active radiation (PAR), also known as photosynthetic photon flux density (PPFD). PAR values were kept constant for southern Africa in this study. This is a reasonable assumption for southern Africa, as it is located beneath the descending limb of the Hadley cell and generally experiences clear weather. This is especially true for winter conditions where 80 % of the days are clear (Cosijn and Tyson, 1996). Consequently, any change in emissions can be accounted for by a change in temperature.

PAR values were either 1000 or 0  $\mu\text{mol}/\text{m}^2\text{s}$ . In MEGAN, PAR values are usually included in an input meteorological file. However, because PAR was kept constant, it was easier to designate PAR values in the FORTRAN code. Initially, constant PAR values were called from the netcdf meteorological file. However, this gave erroneous results. The emission capacity in response to light is derived from PAR values at the top of the atmosphere (TOA) and at the top of the vegetation canopy. MEGAN calculates PAR TOA based on solar angle, and therefore models sunrise and sunset. However, the initial input PAR data would be either 0 or 1000  $\mu\text{mol}/\text{m}^2\text{s}$  for the same hour over the whole of southern Africa (i.e. for the entire model domain). Situations arose at sunrise and sunset where PAR values above the canopy were higher than those at the top of the atmosphere, which is not realistic. Consequently, the light algorithms created unrealistic

and erroneous emission values. To solve this problem, canopy PAR values needed to model sunrise and sunset. This was achieved by altering PAR values in the module gamma\_etc.F, which is called from the megan.F programme (Figure 2.2). PAR was kept constant at  $1000 \mu\text{mol}/\text{m}^2\text{s}$  when the angle between the sun and the horizon is  $10^\circ$  or greater. When the angle of the sun is less than  $10^\circ$  PAR was set to  $0 \mu\text{mol}/\text{m}^2\text{s}$ . The FORTRAN code was also altered to ignore any PAR values in the input meteorological file. Although PAR was kept constant, the emission activity does vary from hour to hour and from summer to winter as the solar angle changes.

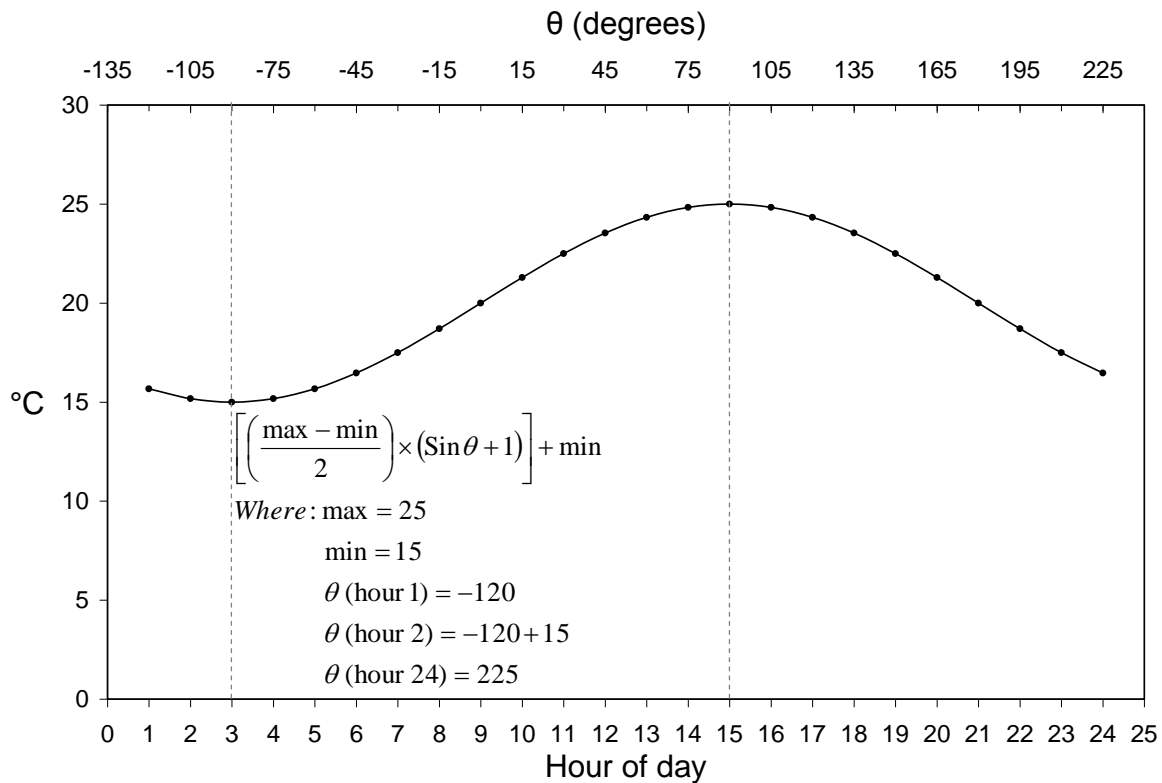


Figure 2.3: Sine wave representing a heating curve of surface temperature. Hourly temperature data was calculated by substituting maximum and minimum CCAM temperatures into the equation for each day. Minimum temperature occurs at 3 am and maximum at 3 pm.

### *Error with Data Time Stamps*

Time stamps of input data need to be in Greenwich Mean Time (GMT). MEGAN then converts GMT to local time based on the longitude of the data. However, the computer



code only calculated time for the Western Hemisphere and not for the Eastern Hemisphere. This code was altered accordingly to include Eastern Hemisphere longitudes.

Furthermore, an error occurred on the time stamp for LAI data. Input meteorology data is in GMT. LAI data for each month is included in the csv file and is not in GMT. Consequently, LAI data for the previous month is used for the first two hours of each month. However, this is inconsequential for emissions estimates as it occurs at night time when the emission activity for light is zero.

### Processing MEGAN output

MEGAN output was converted from  $gs^{-1}$  to  $gm^{-2}month^{-1}$ . MEGAN output gives emission rates for each model grid cell and each hour as  $gs^{-1}$ . However, output needed to be converted to units for a total monthly emission rate and to units that can be compared with previous studies (equations (2.8) to (2.12)). Each model grid cell is about  $3\,600\,000\,000\,m^2$  ( $60\,km^2$ ). Units were converted as follows:

$$\text{MEGAN output units} = \frac{xg}{s \cdot 3\,600\,000\,000\,m^2}$$

Step 1: Sum emission rates for each hour in January

$$\sum_{hour=1}^{744} hour + 1 = \frac{xg}{744s \cdot 3\,600\,000\,000\,m^2} \tag{2.8}$$

Step 2: Convert 744 seconds to one month

1 Month (of 31 days) = 2 678 400 seconds

$$\frac{2\,678\,400\,seconds}{744\,seconds} = 3600 \tag{2.9}$$

$$\frac{3600\,xg}{month \cdot 3\,600\,000\,000\,m^2} \tag{2.10}$$

Step 3: Convert to 1 m<sup>2</sup>

$$\frac{3600 \text{ } / \text{ } 3 \text{ } 600 \text{ } 000 \text{ } 000 \text{ } \text{ x g}}{\text{month} \cdot \text{m}^2} = \frac{1 \times 10^{-6} \text{ x g}}{\text{m}^2 \cdot \text{month}} \quad (2.11)$$

Or step 2 and 3 together:

$$\frac{\text{ x g}}{744 \text{ seconds} \cdot 3 \text{ } 600 \text{ } 000 \text{ } 000 \text{ m}^2} \times 1 \times 10^{-6} = \frac{\text{ g}}{\text{m}^2 \text{ month}} \quad (2.12)$$

### **Quantitative versus Qualitative Methods in Representing Model Uncertainty**

As model inputs change in magnitude so does the model output. A change in model input can be due to a change in physical conditions or due to an error range associated with an input variable. The magnitude of change in an input does not necessarily result in the same magnitude of change in the output. This relationship between change in input and output can be referred to as model uncertainty. Part of the modelling process should answer the question: How does uncertainty in model inputs affect the error in model output? This question can be answered both quantitatively and qualitatively.

In quantitative methods, standard deviations are calculated for individual input variables. If input variables are dependent on each other then a co-variance is calculated. A combined uncertainty of the output is then calculated from the standard deviations of all input variables (Ellison *et al*, 2000). The method described above is difficult to use with this model, because it is not always possible to calculate the standard deviation of input variables. In order to calculate standard deviation you require a sampling size that fits a normal distribution or can be transformed into a normal distribution. Only one of the input variables, namely temperature, fits this description. All other variable are either constant (emission factor and LAI) or only represent two values (Light is either ‘on’ or ‘off’). Furthermore, the error associated with some inputs is thought to be negligible, as will be discussed later, when using a regional model over an extended time period (Otter

*et al*, 2003). As a result, qualitative methods have subsequently been used to represent uncertainty in model output (Guenther *et al*, 2006, Otter *et al*, 2003).

In qualitative methods the error of model output is represented as a factor. For example, Guenther *et al* (2006) ran the model using different sources of data for input and compared the results to a control case. Results ranged from a factor of 0.8 lower to a factor of 4 higher on a global scale. For regional models emissions are estimated to be within a factor of 2 to 3 (Otter *et al*, 2003). Sensitivity analysis in this study will be dealt with in a similar manner.

### **Identifying Areas of 'High' Emission Rates**

When considering FUTURE emission rates it becomes important to identify areas of maximum increase in total isoprene emitted. This often involves finding areas representing peak values of model inputs. To achieve this task objectively the standard deviation of model inputs and outputs will be calculated. The standard deviation can be calculated if the dataset represents a normal distribution (bell shape curve) (Daniel, 1984). One standard deviation is the distance from the mean value in either the positive or negative direction. In other words, the standard deviation in the positive direction represents the mean value of that dataset plus the standard deviation. By definition, one standard deviation in the positive direction splits the dataset into two sections: all values less than or equal to one standard deviation represent 84.13% of the dataset while all values greater than the standard deviation represent 15.87% of the dataset. All values greater than one standard deviation will be used to represent peak values in model inputs and outputs.

## **CHAPTER 3: ISOPRENE EMISSIONS OVER SOUTHERN AFRICA BASED ON CURRENT CLIMATE CONDITIONS**

The aim of this chapter is to demonstrate that isoprene emission estimates for the current climate are reasonable when considering the input data, and in comparison with previous studies. This will be achieved in two ways. Firstly, the spatial distribution of isoprene emission estimates will be presented and compared to a previous study. Secondly, the magnitude of isoprene emission estimates will be considered relative to model inputs and other studies. Isoprene emission estimates based on temperature data from the years 1975 to 2005 will be referred to as **CURRENT**, while estimates based on temperature data from the years 2070 to 2100 are referred to as **FUTURE**.

### **Spatial Distribution of CURRENT Isoprene Emission Rate Estimates**

#### *January CURRENT*

January represents summer conditions when isoprene emissions are expected to be at their highest. Isoprene emission rates for January range from 0- 1.41  $\text{gm}^{-2}\text{h}^{-1}$  and are the result of the isoprene emission factors and emission activity. The distribution of isoprene emission factors for southern Africa demonstrates a north-south gradient, with lower emission factors in the north than in the south (Figure 3.1A). The emission activity of isoprene shows an opposite pattern, with higher emission activity in the north than in the south (Figure 3.1B). Consequently, the resulting distribution of isoprene emission rates is not similar to either the emission factor or emission activity distribution. Instead, peaks in emission rates of isoprene are scattered across the study domain (Figure 3.2A). This pattern can be explained when considering the emission activity in response to photosynthetic active radiation (PAR), temperature and LAI separately, as will be discussed later.

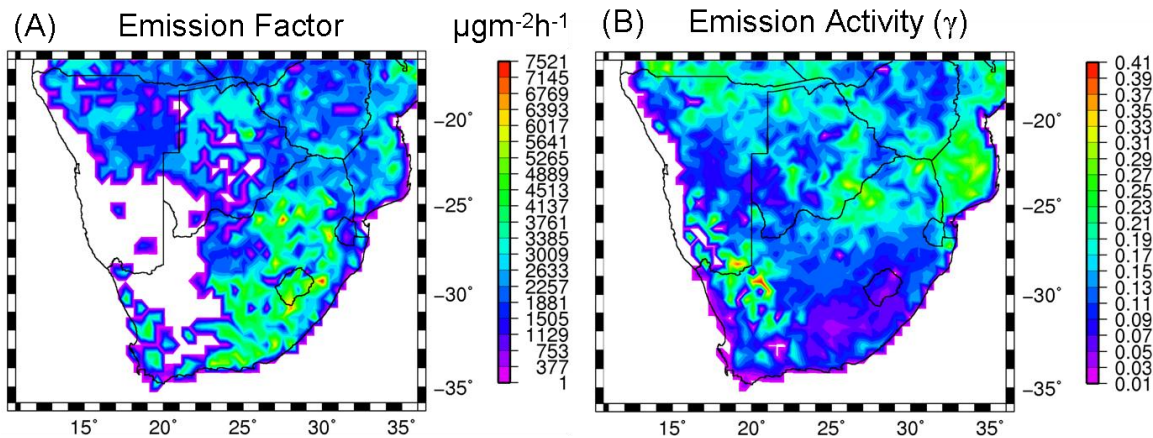


Figure 3.1: (A) Standard isoprene emission factor data used for all months. (B) Isoprene emission activity for January CURRENT calculated as  $\gamma_{Temp} \cdot \gamma_{PPFD} \cdot \gamma_{LAI}$  in equation (2.7).

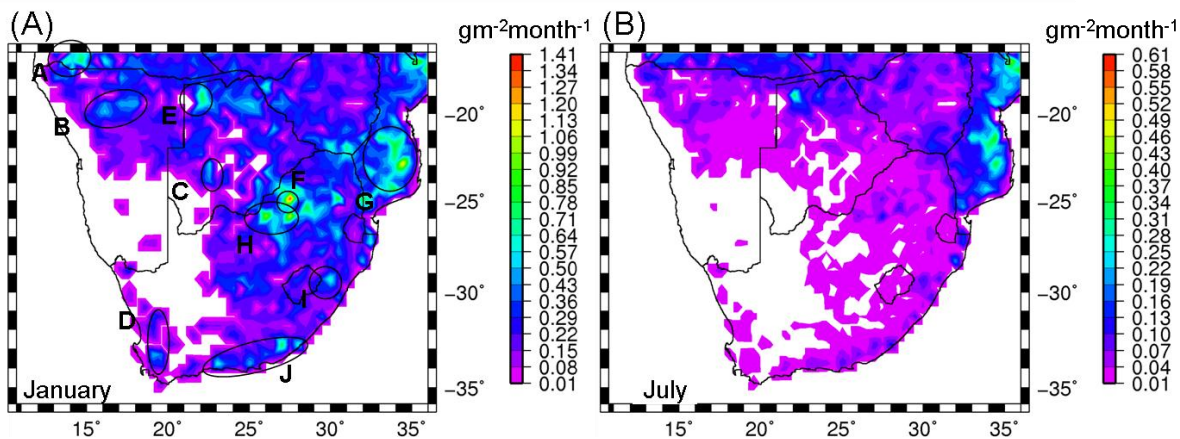


Figure 3.2: Isoprene emission rate estimates for (A) January and (B) July CURRENT in  $gm^{-2}month^{-1}$ .

#### *Driving Variables of Peak Isoprene Emissions*

There are three circumstances that cause peaks in emission rates: areas of high temperature, high temperature and high LAI, and high LAI and high emission factors. Areas of highest temperature correspond well to areas of low LAI (Figure 3.3B and Figure 3.4A). As a result, isoprene emission rates in areas of high temperature are limited by low LAI values, and vice versa. Nevertheless, some peaks in emission estimates can be contributed to high temperatures only. Examples of the three circumstances that cause peaks in emissions can be seen in areas A- J in Figure 3.2A. Area A (Angola West Coast) has relatively low LAI values, yet a peak in isoprene emission rates occurs due to high

temperatures. The same is true for area B (group of peaks in Namibia). Area C (Small peak in Botswana) has similar LAI values to areas A and B, but experiences higher temperatures. Area C also has a lower emission factor, but the high temperatures still cause a peak in isoprene emission rates. Higher temperatures may also be responsible for the peak in area D (Western Cape).

In some cases emission rates are due to relatively high LAI and temperature. These include areas E (Okavango Delta), F (peak near Johannesburg) and G (Mozambique). Emission rates due to high LAI and high emission factors are shown in areas H-J (Gauteng, Mooi River and southern Cape).

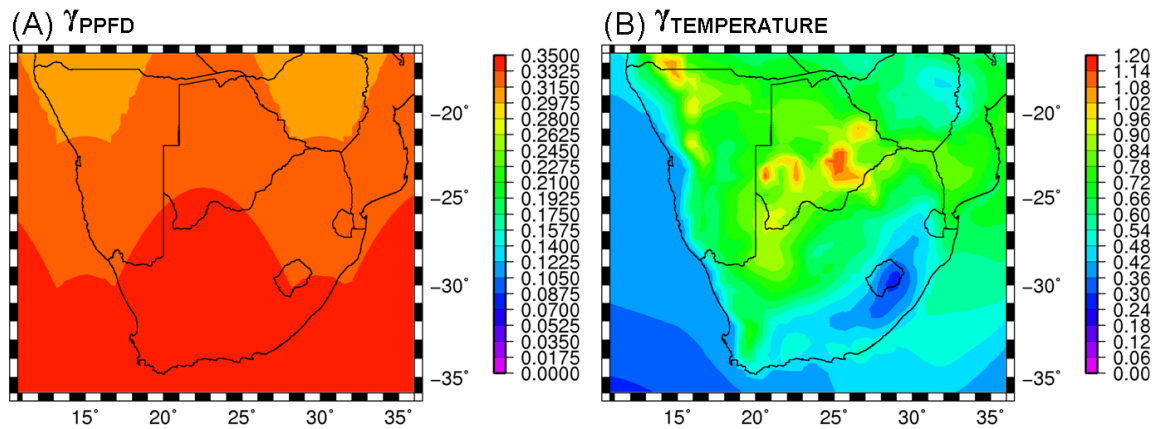


Figure 3.3: January CURRENT average emission activities for (A)  $\gamma_{PPFD}$ , (B)  $\gamma_{TEMP}$ .

PAR is kept constant from day to day and is not responsible for any peaks in emission rates. PAR is used to calculate the emission activity relative to light ( $\gamma_{PPFD}$ ), which varies throughout the day and between seasons. Monthly average PAR emission activity ranges from 0.29- 0.35. The variation in this range is not enough to cause a change in the spatial distribution of emissions. PAR emission activity varies by one percent (Figure 3.3A). However, when multiplied with the emission activity for temperature and LAI as in equation (2.7), the variation accounts for less than one percent variation in emissions. Furthermore, the result of multiplying emission activity of PAR and temperature only, as in equation (2.7), shows the same spatial pattern as the emission activity for temperature (Figure 3.3B and Figure 3.4B). This suggests that PAR does not cause any spatial variation in isoprene emission rates, but only influences the magnitude of emission rates.

This may be due to the method used in incorporating PAR in MEGAN as a constant value.

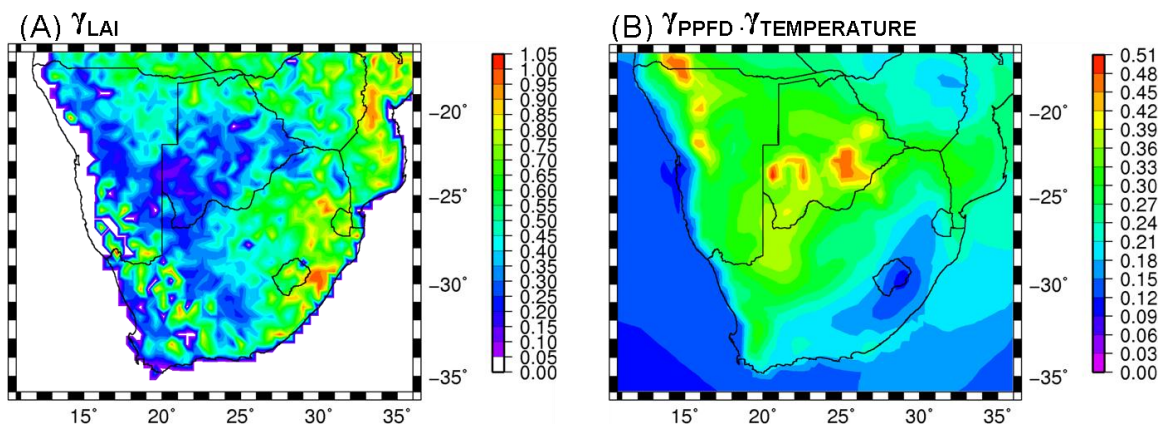


Figure 3.4: January CURRENT average emission activities for (A)  $\gamma_{LAI}$  (no units). PPFD does not change the spatial distribution of emissions as shown in (B) where  $\gamma_{PPFD} \cdot \gamma_{TEMP}$  shows the same distribution as  $\gamma_{TEMP}$  in Figure 3.3B.

### July CURRENT

July isoprene emission rates range from 0- 0.61  $\text{gm}^{-2}\text{h}^{-1}$  (Figure 3.2B). Emissions effectively shut down during July because all physical parameters decrease in the winter months, especially temperature and LAI (Figure 3.5A and Figure 3.6A). The maximum emission activity for average temperature is 0.6 for July compared to 1.2 for January. Furthermore, low temperatures extend across South Africa and are not confined to the escarpment as in January. The highest temperatures no longer occur in Botswana at 23 °S but have moved further north to 17 °S. Emission activity for monthly average PAR ranges from 0.196- 0.28, which is lower in magnitude, but a wider range than January. Unlike January, the spatial variation of PAR in July contributes to the spatial distribution of isoprene emission rates. This is evident when multiplying emission activity of PAR with temperature (Figure 3.6B). If PAR has no effect on the spatial distribution, then  $\gamma_{PPFD} \cdot \gamma_{TEMP}$  in Figure 3.6B would be the same as  $\gamma_{TEMP}$  (Figure 3.5B). Instead, low emission activity values extend into Botswana and over Zimbabwe. The range of emission activity for LAI does not decrease from January to July. However, the spatial extent does decrease.



The highest isoprene emission rates occur over the east coast of Mozambique and over the Okavango Delta in Botswana (Figure 3.2B). LAI remains high in these areas as vegetation thrives on perennial sources of water. Both areas are low-lying and as a result experience warm temperatures all year. A notable increase in LAI occurs over the Western Cape, which is a winter rainfall region. However, temperatures are too low for significant emission estimates. The highest temperatures occur in the north west part of the domain. These temperatures, with LAI values of about 0.5 cause a band of low isoprene emission rates along 17 °S. Emissions are effectively zero south of 22 °S due to low temperatures.

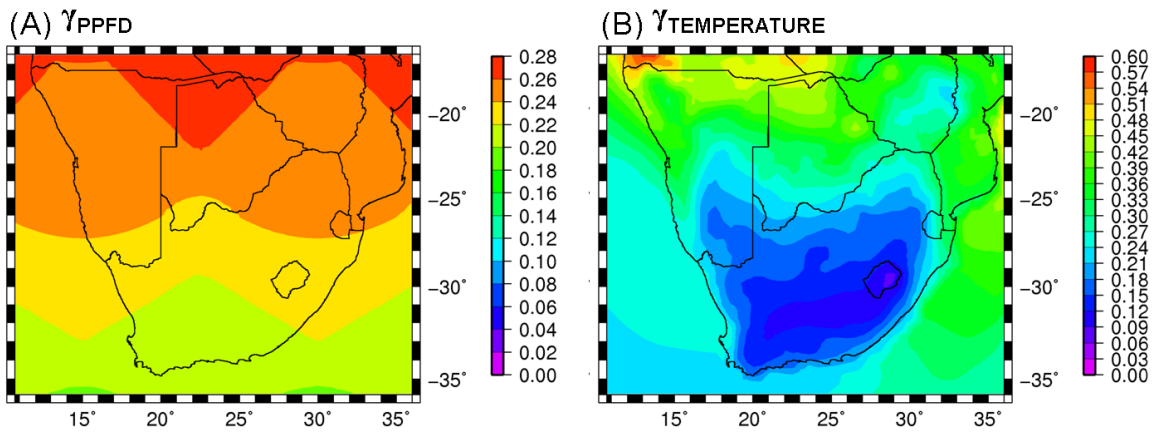


Figure 3.5: July CURRENT average emission response factors for (A)  $\gamma_{PPFD}$  and (B)  $\gamma_{TEMP}$ .

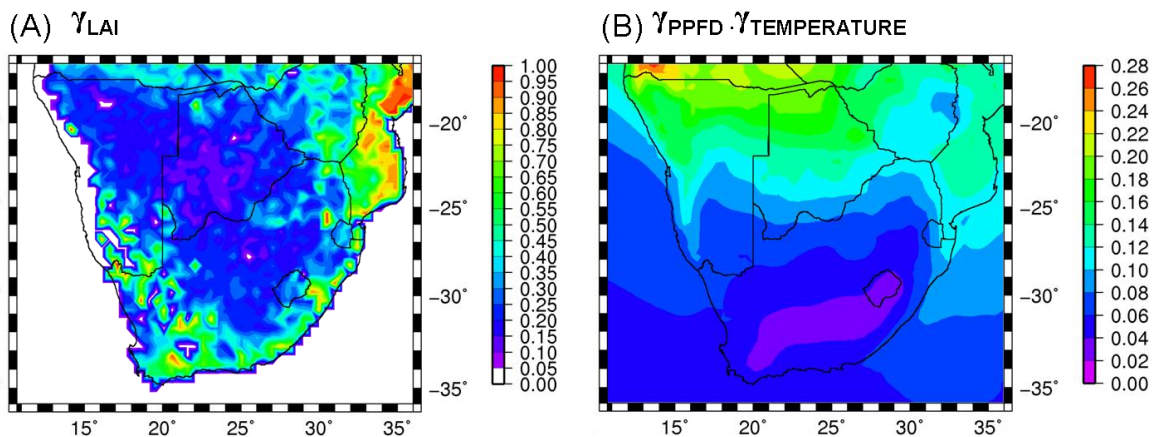


Figure 3.6: July CURRENT average emission response factors for (A)  $\gamma_{LAI}$ . PPFd can effect the spatial distribution of temperature as  $\gamma_{PPFD} \cdot \gamma_{TEMP}$  (B) does not have the same spatial distribution as  $\gamma_{TEMP}$  in Figure 3.5B.



*Comparison of Spatial Distribution of CURRENT Isoprene Emission Rates with a Previous Study*

Guenther *et al* (2006) ran MEGAN at a quarter degree resolution using the same emission factor and LAI data as this study (Figure 3.7A). January estimates show similar areas of peak emissions: the Angola-Namibia border, the north-west interior of South Africa and southern Mozambique (areas A, F, G, and H in Figure 3.7B). However, isoprene emission rates were higher over Mozambique than in this study. The reason for this is that temperatures over Mozambique were higher in the data set used by Guenther *et al* (2006) than in this study.

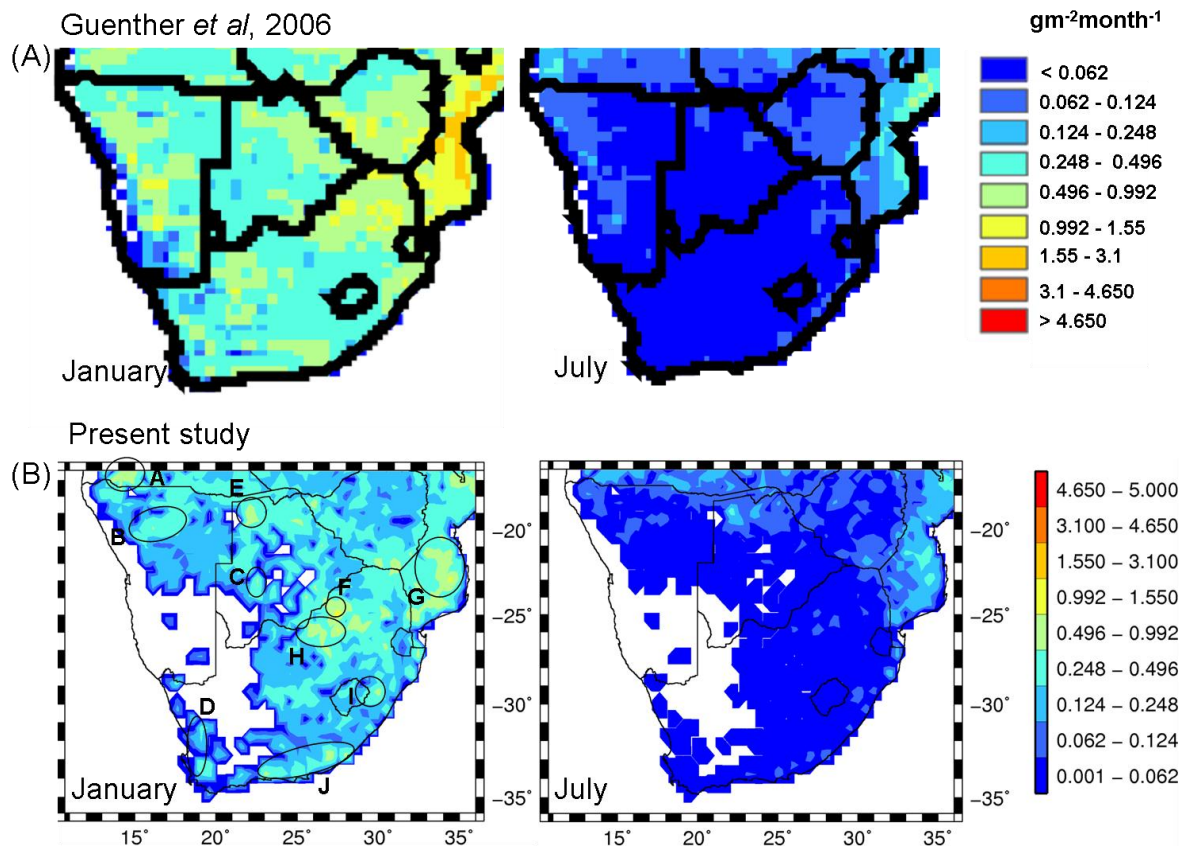


Figure 3.7: (A) Isoprene emission estimates from Guenther *et al* (2006) using the same emission factor and LAI data as this study. (B) Emission rate estimates from this study at the same scale as Guenther *et al* (2006) showing a similar spatial distribution.

July estimates are similar between the two studies, showing the same spatial distribution and peaking around  $0.6 \text{ gm}^{-2}\text{h}^{-1}$ . Peak emissions occur along the north of the domain and

along the Mozambican coast. The similarity in spatial distribution of emissions between the two studies suggests that the model was run correctly for this study. The magnitude of emissions is expected to be different between the two studies as other model variables, like resolution and temperature, are not the same. The emission factor data for this study is missing values for the western part of the domain, accounting for areas of no emissions in Figure 3.7B. That is how the half degree emission factor data from NCAR Community Data Portal (CDP) was originally available.

## **Magnitude of CURRENT Isoprene Emission Rates**

### *Range of Isoprene Emission Rates in Comparison to Previous Studies*

January isoprene emission rates range from 0- 1.41  $\text{gm}^{-2}\text{month}^{-1}$  and July estimates from 0- 0.61  $\text{gm}^{-2}\text{month}^{-1}$ . Otter *et al* (2003) used an earlier version of MEGAN with a resolution of 1km. January estimates ranged from 0- 4.59  $\text{gm}^{-2}\text{month}^{-1}$  and July from 0- 0.986  $\text{gm}^{-2}\text{month}^{-1}$  (Table 3.1). The range of emission rates from Otter *et al* (2003) are higher than this study, which is expected as the spatial resolution of this study is coarser. Otter *et al* (2003), made use of 1km emission factor data which would highlight clusters of small areas of high isoprene emission rates and effectively increase the range of emission rates over an area. This study used half degree emission factor data, which smoothes out small areas of high emission rates into larger areas of average emissions. A difference in model resolution should not affect the total amount of isoprene emitted over a larger area if temperature data is the same. In other words, the total amount of isoprene emitted over the entire model domain would be the same for half degree or 1km emission factor data if identical half degree temperature data is used in both cases. Otter *et al* (2003) did use 1km temperature data. In this case a difference in model resolution will cause emissions over a larger area to be different to a model run at half a degree as temperature data is at a higher resolution and will cause fluctuations in emissions within a half degree cell. However, it will change the range of isoprene emission rates represented in the results. When half degree emission factor data is calculated from 1km data for the model domain, the maximum value changes from 14 194 to 7 536  $\mu\text{g Isoprene m}^{-2}\text{h}^{-1}$ , which is a decrease of about 88 %. However, the magnitude of emissions has the same

order of magnitude. In other words, the higher emission rate is not 10 times greater than the lower emissions rate. This highlights the importance of declaring the spatial resolution when running an emissions model, and considering how that affects the range of model output. In terms of regional atmospheric chemistry, a half degree scale is most likely suitable. Wiedinmyer *et al* (2006) used similar algorithms as MEGAN at a resolution of 1°. July estimates over southern Africa ranged from 0- 0.37 g Isoprene m<sup>-2</sup>month<sup>-1</sup>, which is the same order of magnitude as this study. Guenther *et al* (2006) January estimates ranged from 0.24- 3.1 g Isoprene m<sup>-2</sup>month<sup>-1</sup> and July estimates from 0- 0.992 g Isoprene m<sup>-2</sup>month<sup>-1</sup>. Higher estimates are expected as the spatial resolution is higher; however, estimates are in the same order of magnitude as this study.

Table 3.1: Isoprene emission estimates from this study are the same order of magnitude as previous studies. The units are grams of Isoprene per square meter per month.

		<b>This Study</b>	<b>Otter <i>et al</i>, 2003</b>	<b>Wiedinmyer <i>et al</i>, 2006</b>	<b>Guenther <i>et al</i>, 2006</b>
Horizontal resolution		0.5 degrees	1 km	1 degree	0.25 degrees
Maximum emission rate (gm <sup>-2</sup> month <sup>-1</sup> )	<b>January</b>	1.41	4.59	-	3.1
	<b>July</b>	0.61	0.98	0.37	0.49

#### *Total Isoprene Emitted over the Study Domain*

The isoprene emission totals for January seem to be too low when considering previous studies. Total isoprene emitted over the study domain in January is 0.938 Tg. Otter *et al* (2003) estimated annual isoprene emissions of 56 Tg C (63.4 Tg of isoprene) for Africa south of the equator. This averages out to  $6.2 \times 10^6$  g isoprene/km<sup>2</sup>. If we assume that January emissions occur for six months of the year and July emissions for the other six months, then annual isoprene emissions in this study total 6.8 Tg of isoprene. This equates to  $1.3 \times 10^6$  g isoprene/km<sup>2</sup>, which is 78 % lower than Otter *et al* (2003). It was observed however, that Otter *et al* (2003) included land cover in the tropics, which have higher emission estimates in winter than southern Africa, and therefore contribute a

larger amount to the annual total. However, this alone does not account for the difference in total emissions per km<sup>2</sup>. Unfortunately, no further comparisons can be made between the studies without maps of input variables and emission activities used in Otter *et al* (2003). Both studies use emission factor maps of different spatial resolutions. However, this becomes irrelevant when calculating emissions per km<sup>2</sup> as above. The only other difference between the studies is the input data and the algorithms used. Otter *et al* (2003) used algorithms described by Guenther *et al* (1993) and Guenther *et al* (1999a), whereas this study used algorithms described by Guenther *et al* (2006). A combination of these three factors, winter emissions from tropics, input data and algorithms used, is thought to be responsible for the difference in emissions per km<sup>2</sup>.

#### *Range of Emission Activity in Comparison to Previous Studies*

Daily temperature emission activity ranges from 0.13 - 2.39 for January and 0.04 - 1.4 for July. Emission activity algorithms include a response to hourly and average temperature for the past twenty four hours. Guenther *et al* (2006) plotted emission activity for different average temperatures for the past twenty four hours (Figure 3.8). The emission activity values in this study are reasonable for average temperatures of 280 - 302 K (7- 31 °C) (Figure 3.8). PAR emission activity values ranges from 0 – 0.75 for January and July. LAI emission activity reaches 1.03 for January and 1.01 for July. These ranges for PAR and LAI are reasonable for all scenarios suggested by Guenther *et al* (2006) (Figure 3.8).

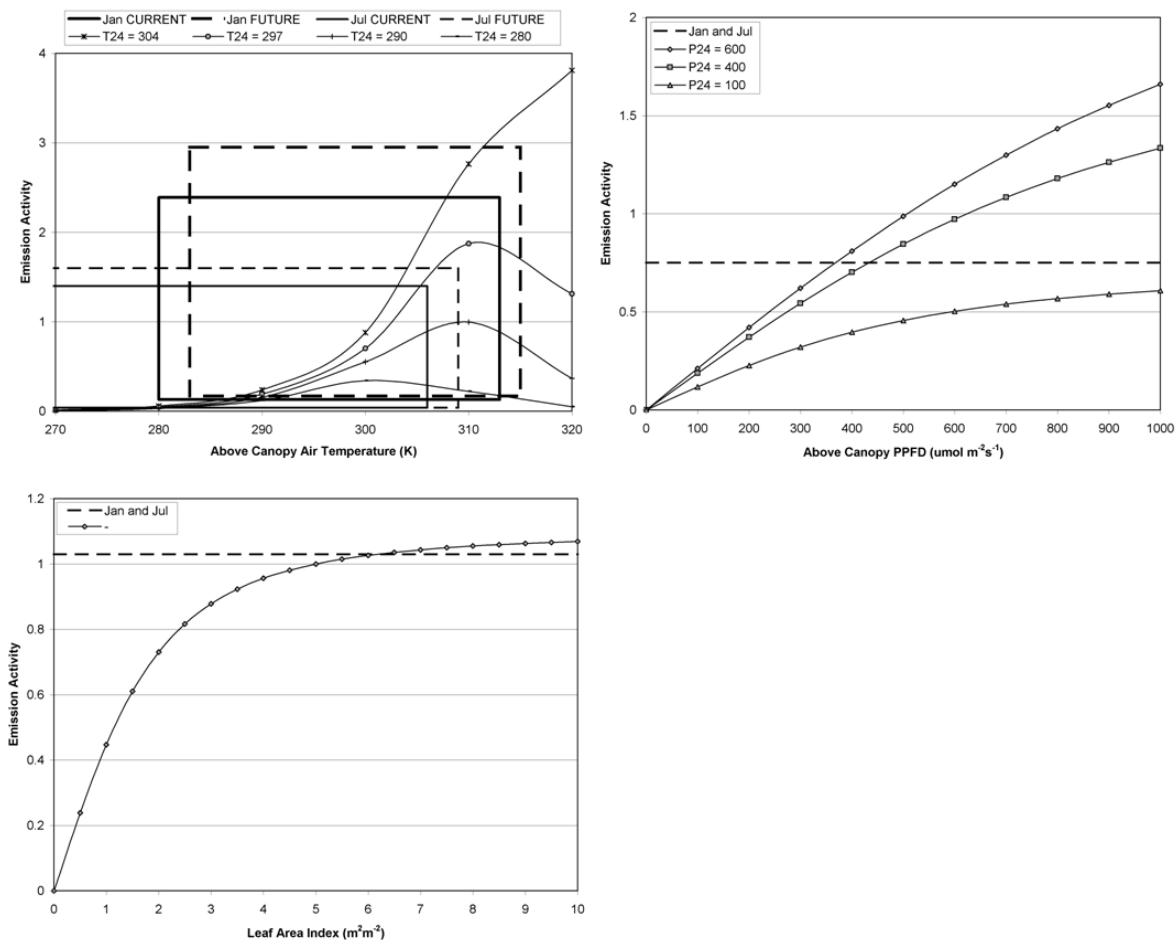


Figure 3.8: Isoprene emission activity values from this study are within the same range of values of scenarios suggested by Guenther *et al* (2006).

### Precautions to Consider when Comparing Independent Model Studies

Although independent model studies may demonstrate similar results it must be emphasised that any modelling study requires some level of verification against observed data. A comparison of model studies should demonstrate that modelers are achieving similar results, which is expected if model algorithms and input parameters like temperature are similar. If model results were not similar then it would suggest that the main driving forces of emissions between models vary considerably and are therefore not representing reality. When results are similar it is an indication that there were no major errors when running the model, for example using the wrong scaling factor or unit for an input variable. However, if both modelers made the same error then we are none the wiser. It must be noted that this is not the case for monoterpene emissions, and it has

been argued in the literature that the reasons for converging modeled isoprene emissions are not the same as those mentioned here (Arneeth *et al*, 2008). Furthermore, a comparison of modelling studies does not suggest that the model results do in fact represent reality.

Model verification would require either a measuring campaign of canopy scale fluxes, as MEGAN estimates canopy scale emission rates in this case, or measurement of canopy ambient air concentrations. For the former, site specific measurements would be taken and compared to half degree model data. Several measurement sites would have to be located within one grid cell of the model domain in order to measure emissions on the same spatial scale as the model. If the landcover type within the model cell is uniform, for example, a pine plantation of similar aged trees, then fewer stations are required. This method for multiple measurements within an area was used by Greenberg *et al*, (1999) who used the relaxed eddy accumulation (REA) technique to measure canopy scale isoprene fluxes over central Africa. REA calculates fluxes based on updraft and downdraft samples (Geron *et al*, 2002, Greenberg *et al*, 2003). The difference in concentration between the two samples determines if the isoprene is from the canopy or from ambient air mixing from above.. Measurements from both summer and winter may not necessarily be required, as a single summer campaign can serve as the model verification data set. If the model is proven to perform well, then it can be assumed that the model performs equally well in winter. It must be noted that the model results from this study are based on average temperature from a thirty year period. It provides the first step towards modeling climate change effects of isoprene in Southern Africa. In order to perform model verification, the model would have to be rerun for the year of observed data. These results do, however, provide good starting points for selecting areas to measure. Furthermore, a measuring campaign can be focused on a smaller area and thus, the model can be refined to a smaller area and a higher resolution. For the latter, ambient air measurements, further analysis of model emission rate will be required in order to convert to concentration. In this case, ambient concentrations can be measured instead of flux measurements.

In addition to canopy scale flux measurements, satellite data can serve as a surrogate to *in situ* measurements. Isoprene concentration can be derived from satellite measurements

of formaldehyde concentration. (Millet *et al*, 2006). However, satellite data, like model data contains its own uncertainty and requires *in situ* verification, as it offer represents total column concentration. Thus, a verification campaign that includes *in situ* measurements, satellite data and model results would provide much insight into modelling of isoprene emissions.

## CHAPTER 4: SENSITIVITY ANALYSIS OF ISOPRENE EMISSIONS TO TEMPERATURE USING CLIMATE CHANGE SCENARIOS

In the previous chapter it was established that the isoprene emission rate estimates for the CURRENT climate scenario (years 1975 to 2005) are reasonable and comparable to previous studies (specifically Guenther *et al*, 2006). Emission rate estimates based on a FUTURE climate scenario (years 2070 to 2100) can now be considered. All model variables for FUTURE scenarios were kept constant except for temperature. Consequently, any changes in emission estimates can be attributed to future temperature scenarios. Whether emissions respond to temperature as expected will be investigated. Once this is established, areas vulnerable to temperature change will be identified. Implications for these areas will then be discussed.

### Introduction

In the previous chapter it was established that the isoprene emission rate estimates for the CURRENT climate scenario (years 1975 to 2005) are reasonable and comparable to previous studies, specifically Guenther *et al*, 2006. This study did not compare favourably with Otter *et al*, 2003, as was discussed, showing a difference in emission of 78 %. Although this difference is large and not comparable, it does not affect the sensitivity analysis covered in this chapter. Sensitivity studies are a measure of model algorithms and equations. It is based on model input and how they affect model output. Thus, although the difference between Otter *et al*, 2003 and this study are large, it is due to a difference in model inputs and model set up. A sensitivity study could support this statement if all model inputs were known for both studies. However, the point here is to demonstrate a sensitivity study based on the emission model algorithms.

### Future Temperature Scenarios

The Conformal-Cubic Atmospheric Model (C-CAM) estimates that the minimum average temperature during the month of January will increase by 2 to 3 °C between 1975 to 2005 and 2070 to 2100 over the study domain (Engelbrecht, 2005). An increase of 4 °C is expected for maximum temperatures over the same time period. Similar increases



are evident over the study domain when comparing average temperature from C-CAM for January CURRENT and January FUTURE (Figure 4.1A). The highest increase in temperature occurs over the western half of the region, ranging from 2.7 to 3.6 °C, while the rest of the region increases between 1.8 and 2.7 °C.

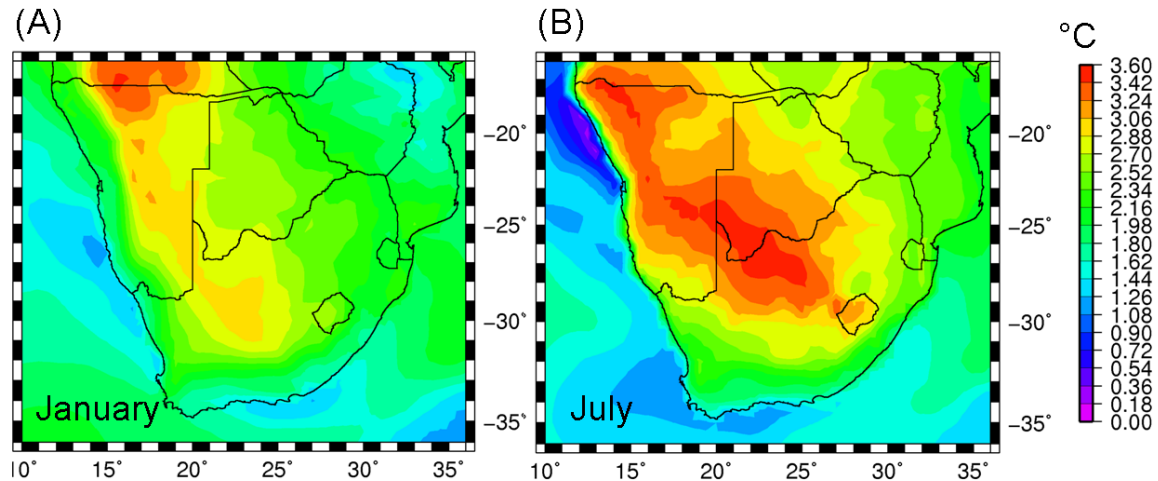


Figure 4.1: Difference in average temperature (°C) from CURRENT to FUTURE for the month of (A) January and (B) July.

### Spatial Distribution of FUTURE Isoprene Emission Rates

It was observed that the spatial distribution of temperature increase (Figure 4.1A) does not change the spatial distribution of emission activity between January CURRENT and January FUTURE (Figure 4.2). The reason for this is that areas of maximum increase in temperature do not coincide with areas of maximum temperature, and therefore do not cause a geographical shift in areas where maximum emission activity due to temperature occurs. Consequently, the spatial distribution of isoprene emission rates is similar between CURRENT and FUTURE scenarios for both January and July (Figure 4.4). Furthermore, areas of maximum increase in temperature do not show a related increase in isoprene emission rate estimates. The reason for this is that these areas coincide with low (zero in most places) emission factors that are associated with dry, sparsely vegetated land cover (Figure 3.1A). However, the magnitude of emission rates over the study domain is higher for FUTURE scenarios. Temperature was found to increase over the study domain for both January and July FUTURE. This caused an increase in magnitude

of the emission activity (Figure 4.2B) and as a result increases isoprene emission rate estimates (Figure 4.4 A and B).

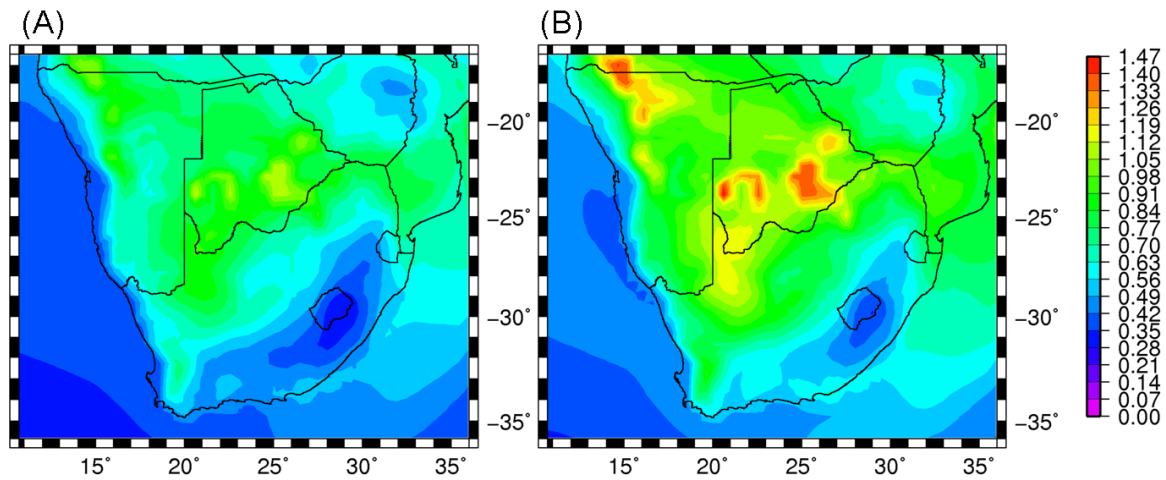


Figure 4.2: Isoprene emission activity (no units) due to temperature for (A) January CURRENT and (B) FUTURE.

### **Regional Totals of Isoprene Emissions and Percent Increase for CURRENT and FUTURE**

Total isoprene emissions for the month of January were found to increase by 34 % from CURRENT to FUTURE scenarios, whilst July emissions increased by 38 % (Table 4.1). However, July emissions were found to be 77 % lower than January emissions for CURRENT and FUTURE scenarios. Since isoprene emissions effectively shut down during the month of July, further discussion in this chapter will be with reference to January emissions. January FUTURE isoprene emission rates range from 0-2.01  $\text{gm}^{-2}\text{month}^{-1}$  compared to CURRENT rates of 0-1.41  $\text{gm}^{-2}\text{month}^{-1}$ .

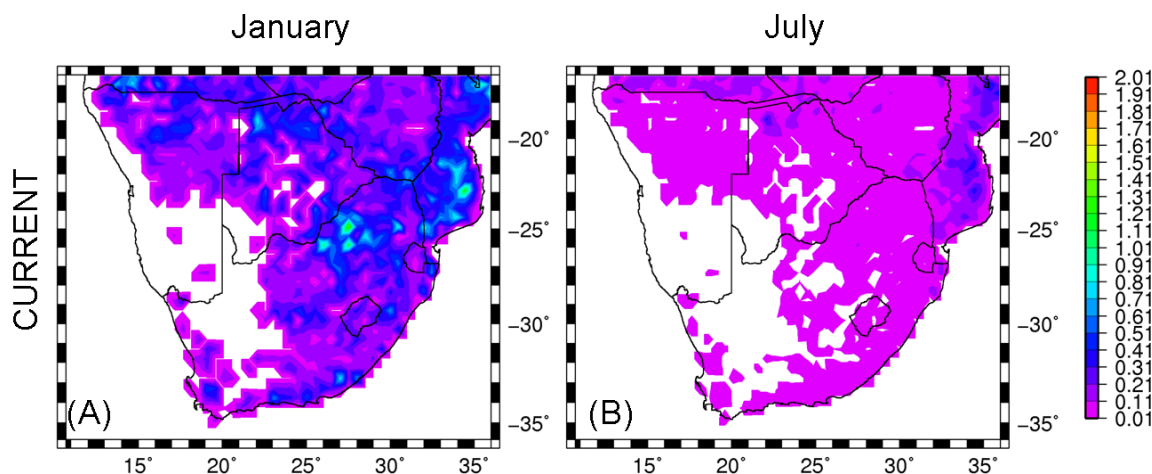


Figure 4.3: Emission rates for the CURRENT climate at the same scale as FUTURE (Figure 4.4) to illustrate the increase in isoprene emissions.

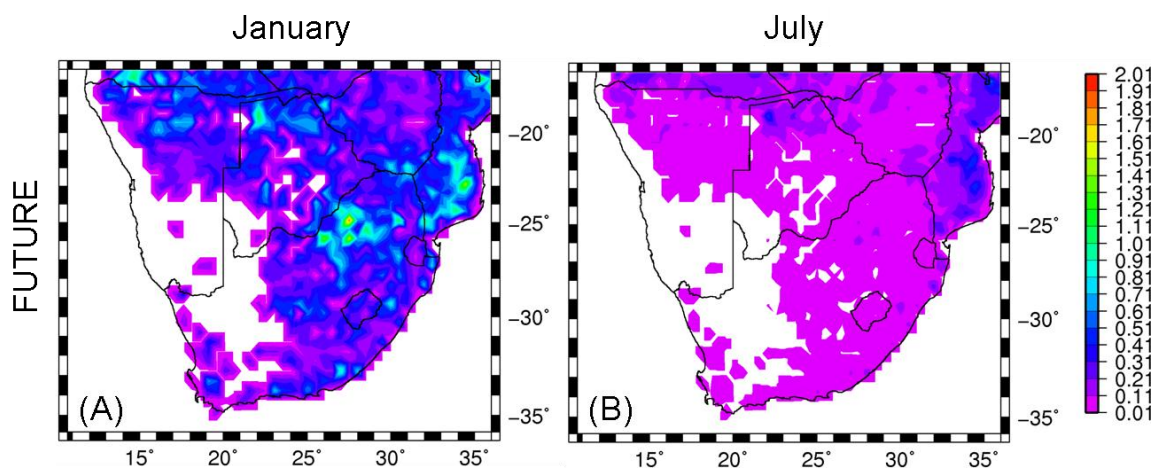


Figure 4.4: Isoprene emission rates ( $\text{gm}^{-2}\text{month}^{-1}$ ) for January and July FUTURE.

Table 4.1: Total monthly isoprene emissions in  $\text{Tg month}^{-1}$ . FUTURE scenarios for January and July show an increase in emissions.

Month	Climate Scenario		Increase	%Increase
	CURRENT	FUTURE		
Jan	0.938	1.259	0.321	34
Jul	0.208	0.289	0.081	38

### *Percentage Increase in Isoprene Emission Rates*

Other studies have modelled emission estimates of isoprene for future climates. These results have been shown to vary more for future climates than results for current conditions. The time difference between current and future scenarios in these studies is generally between 70 to 100 years, although it is not clear what times scale Turner *et al* (1991) used. Global emission models using scenarios of future temperatures and vegetation change for the month of July show isoprene emission rates to increase between 25 and 81 % (Turner *et al*, 1991, Sanderson *et al*, 2003, Wiedinmyer *et al*, 2006, Guenther *et al*, 2006). A regional study of the U.S.A predicted an 81 % increase in isoprene due to temperature (Constable *et al*, 1999). Guenther *et al* (1999) modelled emissions over a sub-tropical savanna region during summer months and estimated a 25 % increase in isoprene emissions due to temperature. This last publication is most relevant to this study as it includes a similar land cover type and is in the same latitudes. The percent increase in emissions is within 9 % of each other (25 % and 34 %) (Table 4.1), which is the same order of magnitude.

### **Sensitivity of Isoprene Emissions to Temperature**

To determine whether isoprene emissions increase with an increase in temperature, it would be more useful to consider the increase in emissions as a percentage. The implications of this increase can then be discussed, after which it would be useful to consider emissions as mass of isoprene emitted.

### *Do Emissions Respond to Temperature as Expected?*

The temperature increase for southern Africa can be split into two regions. The western half of the study domain, where increases of 2.7 to 3.6 °C correspond to emission increases of 40 to 67 %, and the rest of the study domain where increases of 1.8 to 2.7 °C correspond to 10 to 40 % emission increase for the month of January (Figure 4.5A). Overall, January emissions increase between 10 and 67 %, and July emissions between 15 and 60 % in this study. Similar increases have been reported in other studies. Wiedinmyer *et al* (2006) showed increases between 0 and 40 % during July for the same region as this study, using vegetation change and current climate conditions. This

estimate increased to between 0 and 100 % when future temperatures were included. Guenther *et al* (2006) showed emissions to increase by 50 to 100 % during July for the same region as this study using temperature predictions for 2080. Although this study does not include land cover change, it is reassuring that future increases are in the same range as previous studies of the same area.

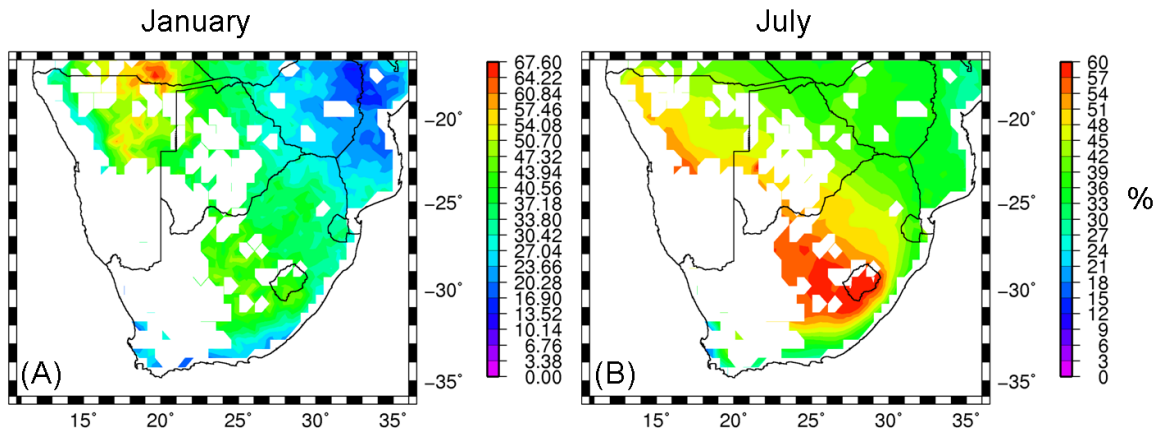


Figure 4.5: Percent increase in emission rates from CURRENT to FUTURE are shown in (A) and (B). Interpolation was not used in this panel, accounting for larger areas of no emissions.

The relationship between temperature and emission activity needs to be re-examined here to understand these increases. The greatest change in emission activity occurs between 18 and 36 °C under standard conditions (Figure 4.6). The rate at which emission activity changes is determined by the other physical parameters like light and average temperature. For example, if the emission activity for light is less than 1, as is the case over southern Africa, then the rate of change will decrease. Average temperature for the past 24 hours affects the gradient slightly differently. Firstly, if average temperature increases, so does the gradient. Secondly, the maximum gradient extends over a wider temperature range. This is likely to be the case over southern Africa as temperature increases are expected in FUTURE scenarios for both minimum and maximum temperatures.

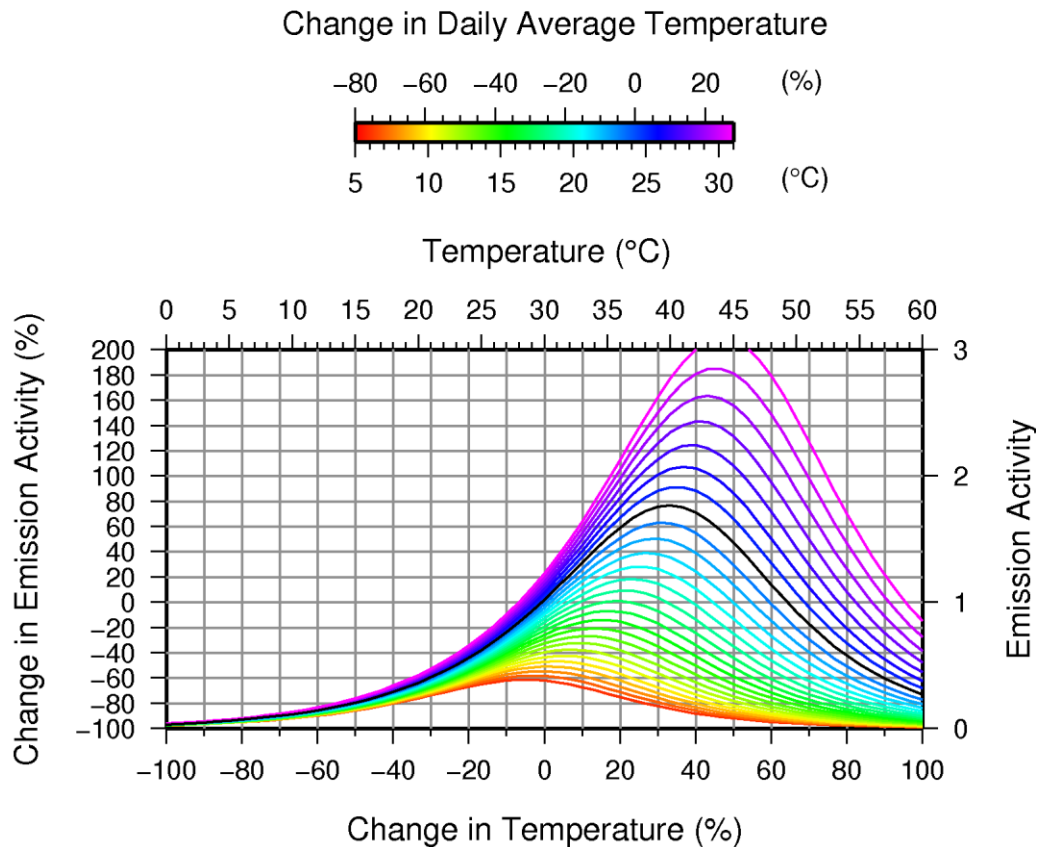


Figure 4.6: Response of isoprene emission activity to temperature. The black line represents standard conditions. Coloured lines represent changes in average temperature for the past 24 hours.

The relationship between temperature and emission activity now needs to be considered for the two regions in the study domain. Three case study areas have been chosen for this purpose. The first is the border between Angola and Namibia (referred to as Ang-Nam from now on) which is situated in the region where future increase in temperature is expected to be the highest (2.7 °C or more). The other two case studies are situated in the region where lower increases in temperature are expected, yet high isoprene emissions of  $0.5 \text{ gm}^{-2}\text{month}^{-1}$  still occur. One of which is the low lying areas of southern Mozambique (referred to as Moz from now on), where temperatures are a bit cooler, but LAI is higher than Ang-Nam. The other is the north east interior of South Africa (referred to as SA from now on) which has slightly cooler temperatures than Mozambique but similar LAI.

It has been estimated that the Ang-Nam region will experience an increase in emissions of about 50 to 60 %. This increase is a reasonable estimate and can be expected for the

region. Given that the future temperature increases by about 3 °C, average temperature will rise accordingly. This will intensify the rate at which emission activity increases according to the response depicted in Figure 4.6. Given these conditions, it is not surprising that average emission activity of about 0.2 increases to about 0.3 from January current to future, causing emission rates to increase by about 50 %. Moz future temperature is estimated to increase by about 2 °C. This will cause an emission factor of 0.25 at 20 °C to increase by 0.09 to 0.34 at 22 °C. The result will be an emissions increase of about 36 %. These values are realistic given the theoretical response of emission activity to temperature depicted in Figure 4.6. To verify that this relationship holds true, the response of emission activity to temperature needs to be determined for each region.

A net increase in temperature from CURRENT to FUTURE scenarios is predicted for all 3 case study regions. Emission activity responds accordingly, increasing in magnitude and in rate of change (Figure 4.7). Ang-Nam experiences the greatest increase in gradient from CURRENT to FUTURE as this region also experiences the greatest increase in temperature. Moz and SA also experience an increase in gradient, but it is less discernable, as increase in temperature is not as great. However, these responses show that emissions respond to temperature as predicted, increasing in magnitude, rate of change and range of temperature over which the greatest rate of change occurs. Areas that are most sensitive to temperature can now be identified. These are not areas that experience the greatest increase in temperature, but rather areas that demonstrate a high emission activity and a significant increase in emission activity (Figure 4.8A). Emission activity cannot be considered by itself as is discussed in the next section. Thus, areas demonstrating maximum increase in mass of isoprene emitted and areas of maximum isoprene emission rates are also considered (Figure 4.8B and Figure 4.9A). The role of emission factors needs to be considered to determine the implications for emission rates over these areas and the region as a whole. This will be dealt with in the next section.

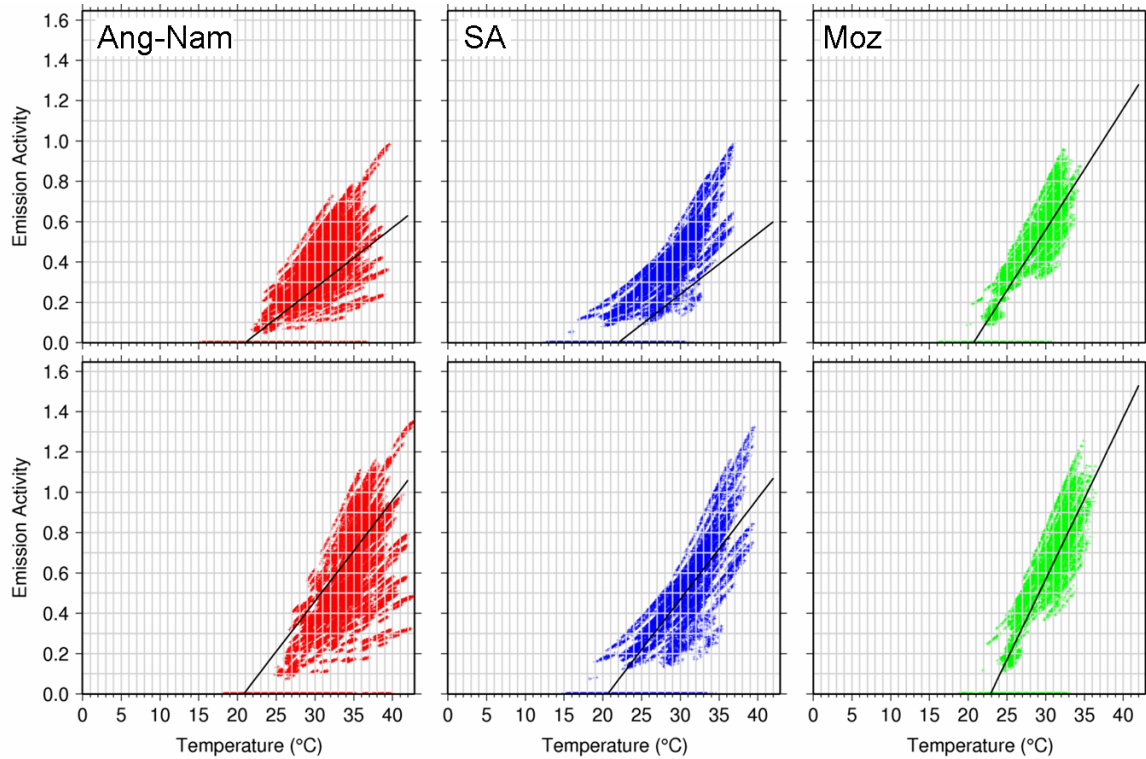


Figure 4.7: The relationship between temperature and emission activity for half degree cells from the three case study areas. Red = Ang-Nam, blue = SA and green = Moz. The top panel represents CURRENT climate and the bottom panel represents the FUTURE climate. Linear regression lines are plotted in black to illustrate an increase in gradient from CURRENT to FUTURE.

Table 4.2: Summary of results shown in Figure 4.7. Ranges are given as min - max (range).

Region	Temperature range (°C)				Emission Activity			
	CURRENT		FUTURE		CURRENT		FUTURE	
Angola/Namibia	22 – 40	(18)	25 – 43	(18)	0.05 – 1	(0.95)	0.1 - 1.35	(1.25)
Mozambique	20 – 34	(14)	22 – 36	(14)	0.1 - 0.95	(0.85)	0.1 - 1.2	(1.1)
SA Interior	17 – 32	(15)	19 – 39	(20)	0.1 – 1	(0.9)	0.1 - 1.3	(1.2)



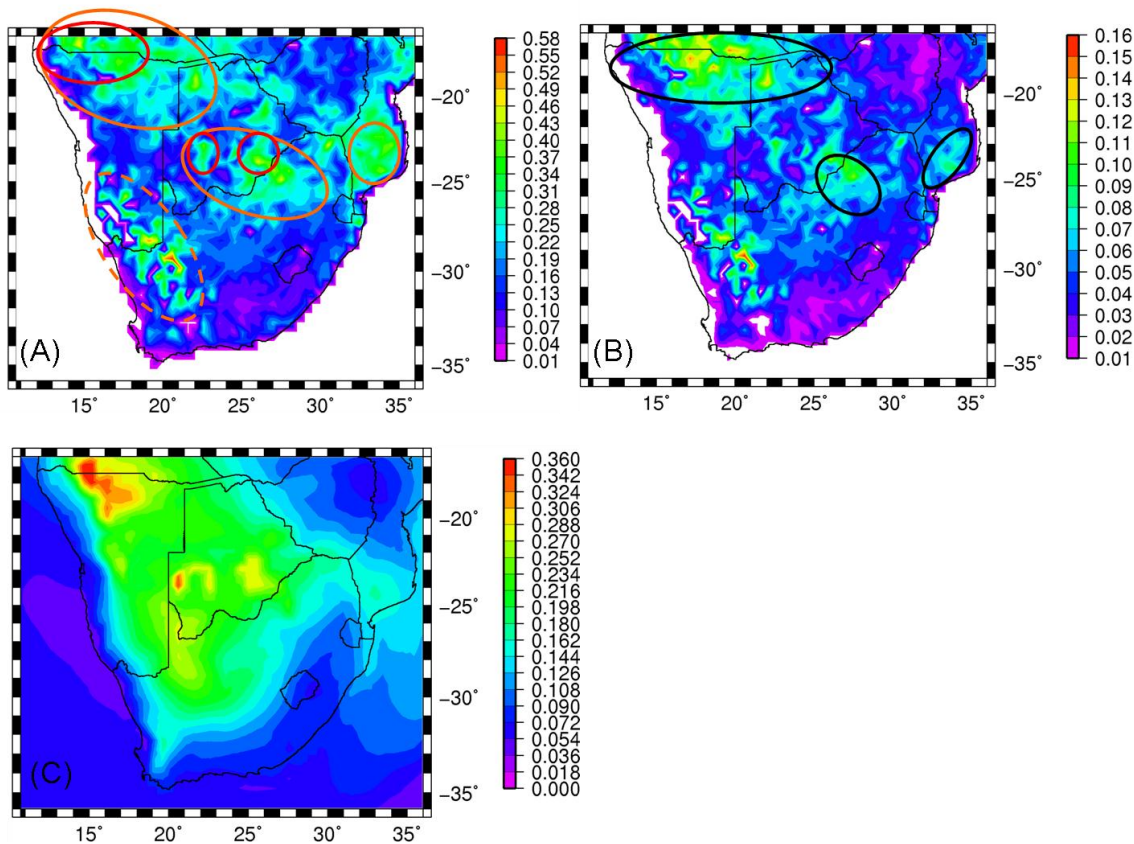


Figure 4.8: (A) Average isoprene emission activity (no units) for January FUTURE. (B) Difference in isoprene emission activity (no units) between January CURRENT and FUTURE. (C) Difference in isoprene emission activity due to temperature (no units) between January CURRENT and FUTURE. Orange ovals represent areas sensitive to temperature based on high emission activity (top left) and high increase in emission activity (top right). The dashed-orange oval is highlighted here but is not discussed in the text because it is associated with very low emission factors. Red ovals highlight areas affected by maximum increase in emission activity due to temperature only (bottom). Black ovals highlight areas of maximum increase in mass of isoprene emitted and highest emission rates.

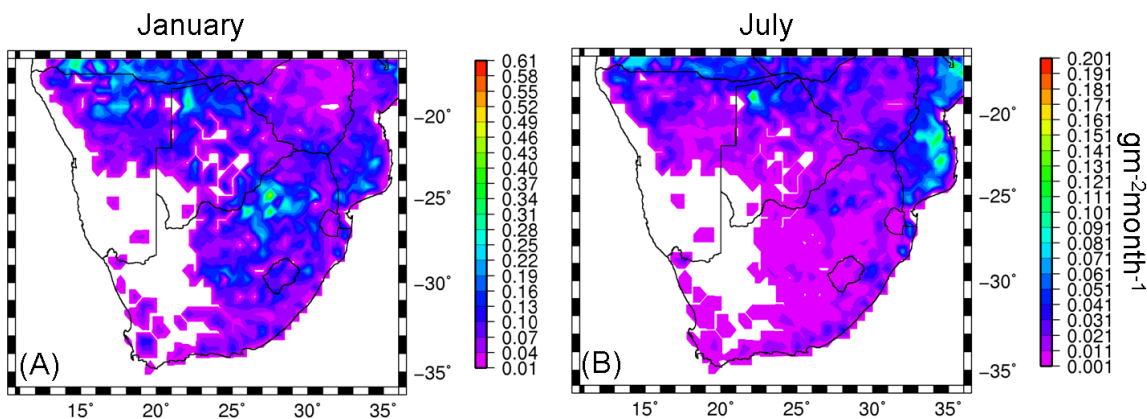


Figure 4.9: Difference in isoprene emission rate estimates (FUTURE - CURRENT) in  $\text{gm}^{-2}\text{month}^{-1}$  for (A) January and (B) July.

*Areas demonstrating high isoprene emission rates and sensitivity to temperature*

Although the approach of using percent increase in emissions is useful in determining whether emission activity responds to temperature as expected, it does have its drawbacks. For example, only the percent increase of the emission activity is known, but not the magnitude. Also, the case occurs where increases represented by large percentages are associated with low values of emission activity. In addition, the emission factor is not taken into account when representing percentage increases in emissions. Regions with low emission factors, like northern Namibia, could double emission rates due to increased emission activity and still be lower than regions with higher emission factors where no or little change in emission activity occurs. Thus, even though all three case study regions show similar ranges of emission activity (Table 4.2), they do not show similar emission rates or percent increase in emissions. This highlights the importance of emission factors in calculating emission rates. Hence, when emission factors are included in identifying areas prone to temperature sensitivity, the three case study areas used earlier are identified (black circles in Figure 4.8B). These areas are important because they experience the highest emission rates and the greatest increase in mass of isoprene emitted.

A more rigorous approach to identifying the case study areas in Figure 4.8B is given here using standard deviations to define areas of high emission activity, change in emission activity, emission rates, change in emission rates and change in temperature emission

activity. The distribution of values for these parameters demonstrates a bell shaped curve, except for change in temperature emission activity which demonstrates a bi-modal distribution. Therefore, one standard deviation is used for all parameters except change in temperature emission activity, for which two standard deviations were used. Areas of high emission activity above one standard deviation and change in emission activity above one standard deviation are shown in Figure 4.10A and correspond to the orange circles in Figure 4.8A. Areas of high emission rates greater than one standard deviation and high increase in emission rates above one standard deviation are shown in Figure 4.10B and correspond to the black circles in Figure 4.8B. Areas of high increase in emission activity due to temperature only above 2 standard deviations are shown in Figure 4.11 and correspond to the red circles in Figure 4.8A. A summary of the standard deviations for each parameter can be found in Table 4.3.

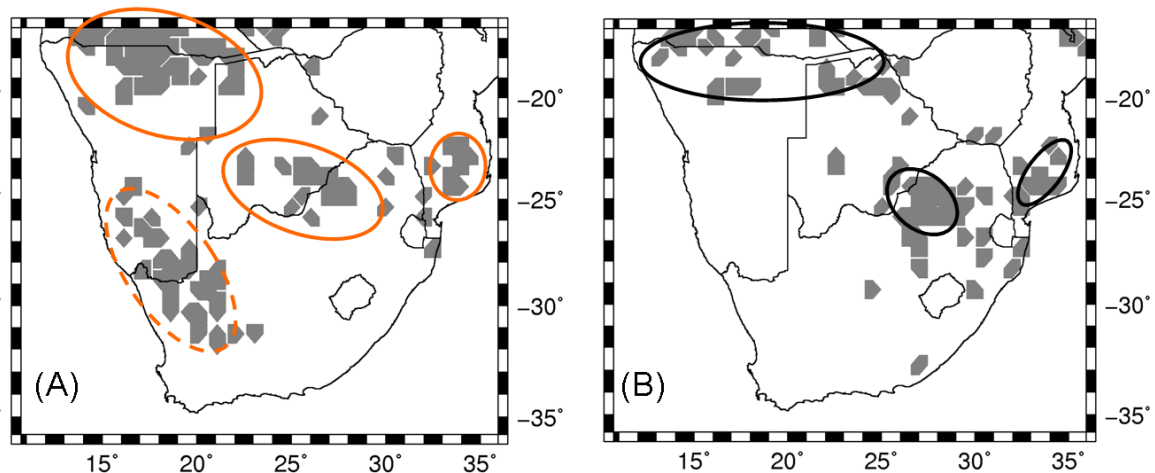


Figure 4.10: (A) Overlay of areas showing highest isoprene emission activity (above 1 standard deviation) and increase in emission activity (above 1 standard deviation). (B) Overlay of areas showing highest isoprene emission rates (above 1 standard deviation) and increase in emission rates (above 1 standard deviation).

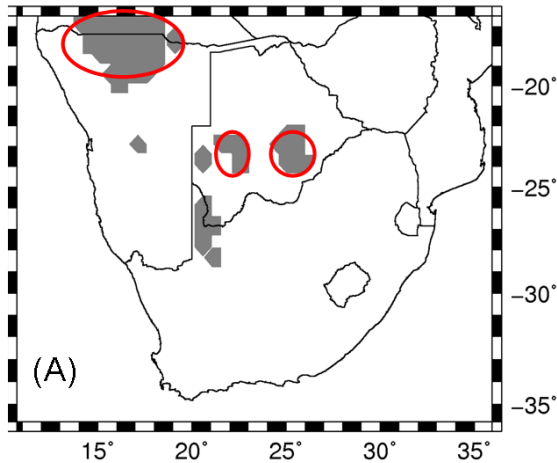


Figure 4.11: Areas showing highest isoprene emission activity due to temperature (above 2 standard deviations).

Table 4.3: Summary of standard deviations used to represent areas in Figure 4.10 and Figure 4.11.

Variable	Std Deviation	No. of std dev	Mean	Mean+Std dev
Emission activity	0.081	1	0.196	0.277
Increase in emission activity	0.020	1	0.047	0.067
Emission rate	0.203	1	0.373	0.576
Increase in emission rates	0.056	1	0.095	0.151
Increase in emission activity due to temperature	0.681	2	0.130	1.492

#### *Other Factors that may affect Sensitivity*

##### *Leaf Area Index*

The response of emission activity to LAI saturates at high LAI values. This is because higher LAI causes shading in the canopy which thus limits emissions. Consequently, the greatest variability in emission activity occurs at lower LAI values between 0 and  $2 \text{ m}^2\text{m}^{-2}$  (Figure 4.12).

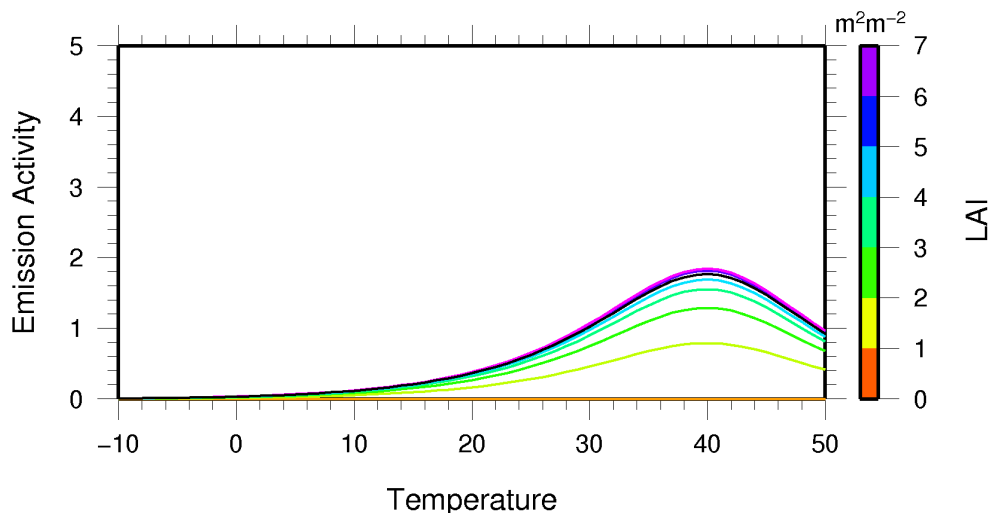


Figure 4.12: Leaf Area Index saturates emission activity from 5  $\text{m}^2\text{m}^{-2}$  but has a greater effect at low values. Black line represents standard conditions.

The highest frequency of LAI over the study domain is from 0.5 to 1.5  $\text{m}^2\text{m}^{-2}$  (Figure 4.13). This range decreases in July, which contributes to the shutting down of isoprene emissions in winter. Seasonal changes in LAI could alter the spatial distribution of emission rates presented in this study. More specifically, areas where LAI is currently between 0.5 and 1.5  $\text{m}^2\text{m}^{-2}$  could increase and cause an increase in emission rates. This includes the case study areas over South Africa, northern Namibia and Angola. It is acknowledged that seasonal changes in LAI were not included in this study and its effect on emissions remains unknown.

#### *Changing Emission Factors due to Changing Land Cover*

Vegetation distribution is expected to change in response to climate change. One such change suggested for southern Africa is bush-encroachment of grasslands (Scholes *et al*, 1999). A direct result of bush-encroachment could be increased emission rates as trees with higher emission factors replace grasses that have lower emission factors. An indirect result of bush-encroachment would be an increase in LAI, effectively increasing emissions. Areas possibly affected by bush encroachment include the case study area over South Africa and extends to the central interior of South Africa. However, it has also been suggested that savanna areas may become less densely vegetated in the west of the region as rainfall decreases (Rutherford *et al*, 1999). This would offset any increases in

emissions due to bush-encroachment. A dynamic vegetation model (DVM) would be needed to estimate future vegetation distribution for all land cover types, and emission factors re-assigned. Inclusion of a DVM was beyond the scope of this study. Furthermore, uncertainty associated with the DVM would have to be calculated and included in the uncertainty associated with emission factor data.

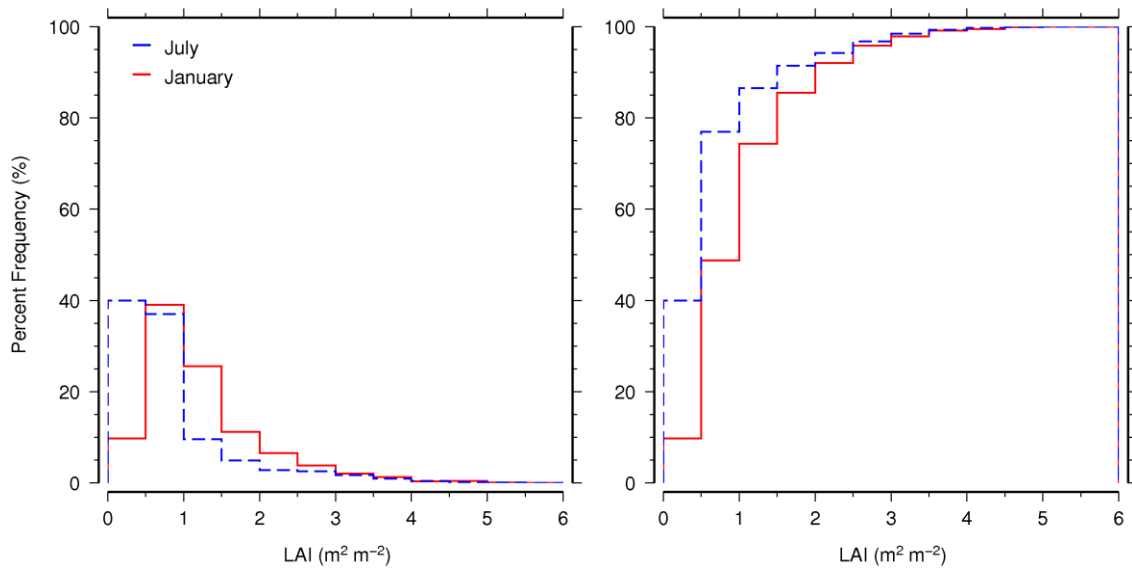


Figure 4.13: Leaf Area Index histogram (left) and cumulative histogram (right) for southern Africa during January and July.

## Summary

In this study emissions have been shown to be sensitive to temperature as expected. Future climatic conditions will increase the variability of isoprene emission rates in response to temperature, and increase the range of temperature that causes the greatest variation in isoprene emissions. However, the realistic implications in terms of the mass of isoprene emitted are not entirely dependent on temperature. Low emission factors and LAI values limit the amount of isoprene emitted. Consequently, important areas in terms of isoprene emitted are identified according to temperature sensitivity, emission factors and LAI. These areas are the three case study regions: The Angola-Namibia border, the north west interior of South Africa and southern Mozambique.

## CHAPTER 5: SUMMARY AND CONCLUSIONS

The results from this study have provided answers to the research aims and objectives set out in Chapter 1. Areas of highest isoprene emission rates have been identified. The driving variables of isoprene emissions have been identified and found to vary from place to place. The sensitivity of isoprene emissions to temperature has been discussed and future emissions have been shown to respond to temperature as expected. However, the results have raised another point of discussion extra to the aims and objectives: Was it beneficial to use regionally downscaled temperature data? A summary of all these points will be given in this chapter, highlighting results from this study.

### **Areas of Highest Isoprene Emissions and Associated Driving Variables**

There were three combinations of driving variables identified which were responsible for peaks in isoprene emission rates. These were:

- high temperatures
- high temperature and high LAI values
- high LAI and high emission factors

Peaks in isoprene emission rate estimates occurred throughout the study domain. Emission rates that appeared to be caused by high temperatures alone occurred in southern Angola, northern Namibia, central Botswana and possibly the Western Cape in South Africa (Areas A, B, C and D in Figure 3.2A). These areas were estimated to emit about  $0.71 \text{ gm}^{-2}\text{month}^{-1}$ .

Emission rates that appeared to be caused by high temperature and high LAI values were identified in the Okavango Delta of Botswana, a small area near Johannesburg and most of Mozambique (Areas E, F and G in Figure 3.2A). These areas were estimated to emit 0.71, 1.41 and  $1.13 \text{ gm}^{-2}\text{month}^{-1}$  respectively.

Finally, emission rates that appeared to be caused by high LAI and high emission factor values all occurred in South Africa. These included the northern interior, and small areas on the east coast and southern Cape coast (Areas H, I and J in Figure 3.2A). These areas were estimated to emit 1.13, 0.71 and 0.71  $\text{gm}^{-2}\text{month}^{-1}$  respectively.

### **Sensitivity of Isoprene Emissions to Increases in Temperature**

Isoprene emission rates based on the future climate scenario showed a similar spatial distribution to estimates based on the current climate scenario. This similarity was slightly unexpected since temperature did not increase uniformly across the study domain. However, the largest increase in temperature occurred over the western half of the study domain, where emission factors were very low, if not zero. Thus, the spatial distribution of isoprene emission rates was similar between the two climate scenarios.

Isoprene emissions were shown to respond to temperature as expected. The future climate scenario predicts an increase in temperature over the study domain. This will cause an increase in daily average temperature, which is used in calculating how isoprene emissions respond to hourly temperature. Consequently, the rate of change of isoprene emissions were estimated to increase as temperature increases. This is due mainly to an increase in daily average temperature. In other words, an increase of 1 °C under future conditions causes a greater increase in isoprene emissions than under current climate conditions (Figure 1.5). Furthermore, the range of temperature, over which the maximum rate of change in emissions occurs, increases (Figure 1.5). This is attributed to the increase in daily average temperature.

To identify areas that are most sensitive to temperature would be to identify areas of a) maximum temperature and b) maximum temperature increase. However, the practical application of modelling isoprene emissions would be to, eventually, include the estimates in an atmospheric chemistry model as a precursor to ozone formation. Thus, a more practical approach would be to consider the sensitivity to temperature of areas that experience the greatest increase in isoprene emission rates and demonstrate high emission rates. Given these criteria, three areas are identified in the study domain. These are the



case study areas highlighted in Chapter 4 (Figure 4.8), the Angola-Namibia border, southern Mozambique and the north-east interior of South Africa.

### **The Use of a Regional Climate Model in Estimating Isoprene Emissions**

Previous studies that estimate future isoprene emissions usually made use of temperature data from general circulation models (GCM) with a 1 degree resolution. This study made use of half degree temperature data from a regional climate model (RCM) which, in theory, could provide a higher resolution and therefore a more accurate spatial distribution of isoprene emission rates. This, however, was not the case. The resolution of the emission factor map had a stronger influence on the range of isoprene emission rate estimates calculated by MEGAN. This was evident when comparing the range of magnitude of emission rates from the current climate with Otter *et al* (2003) and Guenther *et al* (2006). Both publications made use of a finer resolution emission factor map, and consequently had a wider range of emission rates (Table 3.1). This highlights the importance of declaring the resolution at which the emissions model is run. For example, this study used emission factor data that was derived from a data set with a resolution of 1km. However, the model was run at a half degree resolution. The use of finer scale emission factor data will better represent small clusters of areas of high emissions rates. However, it should produce similar results of total isoprene emitted over a larger area when compared to emission model results using a coarser resolution. Yet, it remains to be seen whether the resolution of the emissions model will affect output of an atmospheric chemistry model on a regional scale.

## REFERENCES

- Arneth, A., Monson, R. K., Schurgers, G., Niinemets, Ü., and Palmer, P. I., 2008 Why are estimates of global isoprene emissions so similar (and why is this not so for monoterpenes)?, *Atmospheric Chemistry and Physics*, 8, 4605-4620.
- Atkinson, R., Atmospheric Chemistry of VOCs and NO<sub>x</sub>, 2000, *Atmos., Envir.*, 34, 2063-2101.
- Berry, M., Lioy, P. J., Gelperin, K., Buckler, G. and Klotz, J., 1991, Accumulated exposure to ozone and measurement of health effects in children and counselors at two summer camps, *Environmental Research*, 54:2, 135-150.
- Chameides, W., L., Lindsay, R., W., Richardson, J. and Kiang C., S., 1988, The role of Biogenic Hydrocarbons in Urban Photochemical Smog: Atlanta as a Case Study, *Science*, 241, 1473-1475.
- Chen, T., Gokhale, J., Schofer, S. and Kuschner, W. G., 2007, Outdoor Air Pollution: Ozone Health Effects, *The American Journal of Medical Sciences*, 333:4, 244-248.
- Constable, J. V. H., Guenther, A. B., Schimel, D. S., Monson, R. K., 1999, Modelling changes in VOC emission in response to climate change in the continental United States, *Global Change Biology*, 5, 791-806.
- Cosijn, C. and Tyson, P. D., 1996, Stable discontinuities in the atmosphere over southern Africa, *South African Journal of Science*, 92, 381-396.
- Daniel, W. W., 1984, *Essentials of Business Statistics*, Houghton Mifflin Company, Boston, pp 93-99.
- Davidson, C. I., Phalen, R. F. and Solomon, P. A., 2005, Airborne Particulate Matter and Human Health: A Review, *Aerosol Science and Technology*, 39, 737-749.
- Dickerson, R. R., Stedman, D. H. and Delany, A. C., 1982, Direct measurements of ozone and nitrogen dioxide photolysis rates in the troposphere, *Journal of Geophysical Research*, 87, 4933-4946.
- Ellison, S., Rosslein, M. and Williams, A., 2000 ed, *Quantifying Uncertainty In Analytical Measurement*, 2<sup>nd</sup> Edition, EURACHEM/CITAC, UK, pp. 25-27.
- Engelbrecht, F., 2005, Simulations of Climate and Climate Change over Southern and Tropical Africa with the Conformal-Cubic Atmospheric Model. In: Schulze, R.E. (Ed) *Climate Change and Water Resources in Southern Africa: Studies on Scenarios, Impacts, Vulnerabilities and Adaptation*. Water Research Commission, Pretoria, RSA, WRC Report 1430/1/05. Chapter 4, pp 57-74

- Friedrich, R. and Obermeier, A., 1999, Anthropogenic emissions of volatile organic compounds, In: Hewitt, C. N., (ed), *Reactive Hydrocarbons in the Atmosphere*, Academic, San Diego, Calif, 2 - 39.
- Geron, C. D., Guenther, A. B., Sharkey, T. D. and Arnts, R. R., 2000, Temporal variability in basal isoprene emission factor, *Tree Physiology*, 20, 799-805.
- Geron, C. D., Guenther, A. B., Greenberg, J. P., Loesher, H. W., Clark, D., and Barker, B., 2002, Biogenic volatile organic compound emissions from lowland tropical wet forest in Costa Rica, *Atmospheric Environment*, 36, 3 793-3 802.
- Greenberg, J. P., Guenther, A. B., Madronich, S., Baugh, W., Ginoux, P., Druilhet, A., Delmas, R. and Delon, C., 1999, Biogenic volatile organic compound emissions in central Africa during the Experiment for the Regional Sources and Sinks of Oxidants (EXPRESSO) biomass burning season, *Journal of Geophysical Research*, 104, 30 659- 30 672.
- Greenberg, J. P., Guenther, A. B., Harley, P., Otter, L., Veenendl, E. M., Hewitt, C. N., James, A. E., and Owen, S. M., 2003, Eddyflux and leaf-level measurements of biogenic VOC emissions from mopane woodland of Botswana, *Journal of Geophysical Research*, 108, doi 10.1029/2002JD002317.
- Guenther, A., Zimmerman, P., Harley, P., Monson, R. K. and Fall, R., 1993, Isoprene and monoterpene emission rate variability: model evaluations and sensitivity analyses, *Journal of Geophysical Research*, 98, 12 609-12 617.
- Guenther, A., Hewitt, C. N., Erickson, D., Fall, R., Geron, C., Graedel, T., Harley, P., Klinger, L., Lerdau, M., McKay, W., A, Pierce, T., Scholes, B., Steinbrecher, R., Tallamraju, R., Taylor, J. and Zimmerman, P., 1995, A global model of natural volatile organic compound emissions, *Journal of Geophysical Research*, 100, 8 873-8 892.
- Guenther, A., Baugh, B., Grasseur, G., Greenberg, J., Harley, P., Klinger, L., Serça, D. and Vierling, L., 1999a, Isoprene emission estimates and uncertainties for the Central African EXPRESSO study domain, *Journal of Geophysical Research*, 104, 30 625-30 639.
- Guenther, A. B., Archer, S., Greenberg, J., Harley, P., Helmig, D., Klinger, L., Vierling, L., Wildermuth, M., Zimmerman, P. and Zitzer, S., 1999b, Biogenic hydrocarbon emissions and land use/climate change in a sub-tropical savanna, *Phys., Chem., Earth*, 24, 659-667.
- Guenther, A., Geron, C., Pierce, T., Lamb, B., Harley, P. and Fall, R., 2000, Natural emissions of non-methane volatile organic compounds, carbon monoxide, and oxides of nitrogen from North America, *Atmospheric Environment*, 34 2205 - 2230.

- Guenther, A., Karl, T., Harley, P., Wiedinmyer, C., Palmer, P., I. and Geron, C., 2006, Estimates of global terrestrial isoprene emissions using MEGAN (Model of Emissions of Gases and Aerosols from Nature), *Atmospheric Chemistry and Physics*, 6, 3 181-3 210.
- Haagen-Smit, A. J., 1952, Chemistry and Physiology of Los Angeles Smog, *Industrial and Engineering Chemistry*, 44, 1 342-1 346.
- Hansen, M., DeFries, R. S., Townshend, J. R. G., Carroll, M., Dimiceli, C., and Sohlberg, R. A., 2003, Global Percent Tree Cover at a Spatial Resolution of 500 Meters: First Results of the MODIS Vegetation Continuous Fields Algorithm, *Earth Interactions*, 7(10), 1–15.
- Harley, P., Guenther, A. and Zimmerman, P., 1996, Effects of light, temperature and canopy position on net photosynthesis and isoprene emission from sweetgum (*Liquidambar styraciflua*) leaves, *Tree Physiology*, 16, 25-32.
- Harley, P., Guenther, A. and Zimmerman, P., 1997, Environmental controls over isoprene emission in deciduous oak canopies, *Tree Physiology*, 17, 705-714.
- IPCC, 2000, *Special Report on Emission Scenarios*, Nakicenovic, N., Alcamo, J., Davis, G., de Vries, B., Fenhann, J., Gaffin, S., Gregory, K., Grübler, A., Yong Jung, T., Kram, T., Lebre La Rovere, E., Michaelis, L., Mori, S., Morita, T., Pepper, W., Pitcher, H., Price, L., Riahi, K., Roehrl, A., Rogner, H., Sankovski, A., Schlesinger, M., Shukla, P., Smith, S., Swart, R., van Rooijen, S., Victor, N. and Dadi, Z, Cambridge University Press, Cambridge.
- IPCC, 2001, *Climate Change 2001: The Scientific Basis*, Contribution of Working Group I to the Third Assessment Report of the Intergovernmental Panel on Climate Change (IPCC), edited by J., T., Houghton, Y., Ding, D., J., Griggs, M., Noguer, P., J., van der Linden, and D., Xiaosu, Cambridge University Press, Cambridge, pp 351-406.
- Kanakidou, M., Seinfeld, J. H., Pandis, S. N., Barnes, I., Dentener, F. J., Facchini, M. C., van Dingenen, R., Ervens, B., Nenes, A., Nielsen, C. J., Swietlicki, E., Putaud, J. P., Balkanski, Y., Fuzzi, S., Horth, J., Moortgat, G. K., Winterhalter, R., Myhre, C. E. L., Tsigaridis, K., Vignati, E., Stephanou, E. G. and Wilson, J., 2004, Organic aerosol and global climate modelling: a review, *Atmospheric Chemistry and Physics Discussions*, 4, 5855-6024.
- Karl, T., Fall, R., Rosenstiel, T. N., Prazeller, P., Larsen, B., Seufert, G. and Lindinger, W., 2002, On-line analysis of the <sup>13</sup>CO<sub>2</sub> labeling of leaf isoprene suggests multiple subcellular origins of isoprene precursors, *Planta*, 215: 894-905.
- Klawatsch-Carrasco, N., Doussin, J. F. and Carlier, P., 2004, Absolute rate constants for the gas-phase ozonolysis of isoprene and methylbutenol, *Int. J. of Chemical Kinetics*, 36, 152-156.

- Klinger, L., F., Greenberg, J., Guenther, A., Tyndall, G., Zimmerman, P., M'Bangui, M., Moutsambote, J. and Kenfack, D., 1998, Patterns of volatile organic compound emissions along a savanna-rainforest gradient in central Africa, *Journal of Geophysical Research*, 103, 1443- 1454.
- Lathiére, J., Hauglustaine, D. A., Friend, A., De Noblet-Ducoudré, N., Viovy, N. and Folberth, G., 2005, Impact of climate variability and land use changes on global biogenic volatile organic compound emissions, *Atmospheric Chemistry and Physics Discussions*, 5, 10613-10656.
- Leliaert, F., Bond, W. and Midgley, G. F., 2003, What Controls South African Vegetation - climate or fire?, *South African Journal of Botany*, 69 (1), 79-91.
- Lerdau, M., Guenther, A. and Monson, R., 1997, Plant production and emission of volatile organic compounds, *Bioscience*, 47, 373-383.
- Lippmann, M., 1989, Health effects of ozone: A critical review, *International Journal of Air Pollution Control and Waste Management*, 39:5, 672-695.
- Loreto, F. and Sharkey, T., 1990, A gas-exchange study of photosynthesis and isoprene emission in *Quercus rubra* (Northern Red Oak) L., *Planta*, 182, 523-531.
- McKee, D. J., 1993, *Tropospheric Ozone: Human health and agricultural impacts*, CRC Press Inc., U.S.A.
- McMurry, J., 2007, *Organic chemistry: a biological approach*, Belmont CA, Thomson Brooks/Cole.
- Millet, D., Jacob, D., Turquety, S., Hudman, R., Wu, S., Fried, A., Walega, J., Heikes, B., Blake, D., Singh, H., 2006, Formaldehyde distribution over North America: Implications for satellite retrievals of formaldehyde columns and isoprene emission, *Journal of Geophysical Research*, 111:D24S02
- Monson, R. K. and Fall, R., 1989, Isoprene emission from Aspen leaves, *Plant Physiol.*, 90, 267-274.
- Monson, R. K., Jaeger, C. H., Adams, W. W., Driggers, E. M., Silver, G. M. and Fall, R., 1992, Relationships among Isoprene Emission Rate, Photosynthesis, and Isoprene Synthase Activity as Influenced by Temperature, *Plant Physiol.*, 98, 1175-1980.
- Muller, J., 1992, Geographical distribution and seasonal variation of surface emissions and deposition velocities of atmospheric trace gases, *J. Geophys. Res.*, 97, 3787-3804, 1992.
- Otter, L., Guenther, A., Wiedinmyer, C., Fleming, G., Harley, P. and Greenberg, J., 2003, Spatial and temporal variations in biogenic volatile organic compound emissions for Africa south of the equator., *Journal of Geophysical Research*, 101., doi: 10.1029/2002JD002609.

- Piccot, S. D., Watson, J. J. and Jones, J. W., 1992, A global inventory of volatile organic compound emissions from anthropogenic sources, *J. Geophys. Res.*, 97, 9897-9912, 1992.
- Pienaar, J. J. and Helas, G., 1996, The kinetics of chemical processes affecting acidity in the atmosphere, *South African Journal of Science*, 92, 128-132.
- Rosenstiel, T. N., Potosnak, M. J., Griffin, K. L., Fall, R. and Monson, R. K., 2003, Increased CO<sub>2</sub> uncouples growth from isoprene emission in an agriforest ecosystem, *Nature*, 421, 256-259.
- Rutherford, M. C., Powrie, L. W. and Schulze, R. E., 1999, Climate Change in conservation areas of South Africa and its potential impact on floristic composition: a first assessment, *Diversity and Distributions*, 5, 253-262.
- Rutherford, M. C., O'Farrel, P., Goldberg, K., Midgley, G. F., Powrie, L. W., Ringrose, S., Mattheson, W. and Timberlake, J., 2000, *SAFARI 2000: Subproject 6: Species composition of southern African vegetation*, NBI Rep., DACST, Pretoria, S., Africa.
- Sanadze, G. A., 1966, On the mechanism of diene (C<sub>5</sub>H<sub>8</sub>) production in illuminated leaves, *Fiziol., Rast.*, 13, 753-760.
- Sanadze, G. A., 1991, Isoprene Effect-Light Dependent emission of isoprene by green part of plants, In: Sharkey, T. D., Holland, E. A. and Mooney, H. A., (eds), *Trace gas emission from plants*, Academic Press, San Diego, 135-150.
- Sanderson, M., G., Jones, C., D., Collins, W., J., Johnson, C., E. and Derwent, R., G., 2003, Effect of Climate Change on Isoprene Emissions and the Surface Ozone Levels, *Geophysical Research Letters*, 30, 1-4.
- Scholes, R. J., Midgley, G. F. and Wand, S. J. E., 1999, *The Vulnerability and adaptation of rangelands*, South African Climate Change Country Studies Contract Report, Division of Water, Environment and Forest Technology, CSIR, Pretoria, 1-19.
- Seaten, A., Godden, D., MacNee, W. and Donaldson, K., 1995, Particulate Air Pollution and acute health effects, *The Lancet*, 345, 176-178.
- Seinfeld, J., H. and Pandis, S. N., 1998, *Atmospheric Chemistry and Physics: From Air Pollution to Climate Change*, John Wiley and sons, Inc, United States of America.
- Sharkey, T. D., Loreto, F., Delwiche, C. F., 1991, High carbon dioxide and sun/shade effects on isoprene emission from oak and aspen leaves, *Plant, Cell and Environment*, 14, 333-338.
- Sharkey, T. D., Singsaas, E. L., Vanderveer, P. J. and Geron, C., 1996, Field measurements of isoprene from trees in response to temperature and light, *Tree Physiology*, 16, 649-654.

- Sharkey, T. D., Wiberely, A. E. and Donohue, A. R., 2007, Isoprene emissions from plants: why and how, *Annals of Botany*, doi:10.1093/aob/mcm240.
- Silver, G. and Fall, R., 1991, Enzymatic synthesis of isoprene from dimethylallyl diphosphate in Aspen leaf extracts, *Plant Physiol.*, 97, 1588-1591.
- Silver, G. M. and Fall, R., 1995, Characterisation of Aspen isoprene synthase, an enzyme responsible for leaf isoprene emission to the atmosphere, *The Journal of Biological Chemistry*, 270, 13 010-13 016.
- Singsaas, E. L. and Sharkey, T. D., 2000, Relationships among Isoprene Emission Rate, Photosynthesis, and Isoprene Synthase Activity as Influenced by Temperature, *Plant, Cell and Environment*, 23, 751-757.
- Stull, R. B., 2000, *Meteorology for Scientists and Engineers*, Brookes/Cole, U.S.A, pp312, 316.
- Thunis, P. and Cuvelier, C., 2000, Impact of biogenic emissions on ozone formation in the Mediterranean area - a BEMA modelling study, *Atmospheric Environment*, 34, 467-481.
- Trainer, M., Williams, E. J., Parrish, D. D., Buhr, M. P., Allwine, E. J., Westberg, H. H., Fehsenfeld, F. C. and Liu, S. C., 1987, Models and observations of the impact of natural hydrocarbons on rural ozone, *Nature*, 329, 705-707.
- Turner, D. P., Baglio, J. V., Wones, A. G., Pross, D., Vong, R., Mcveety, B. D., Phillips, D. L., 1991, Climate change and isoprene emissions from vegetation, *Chemosphere*, 23, 37-56.
- Twomey, S., 1977, The influence of pollution on the shortwave albedo of clouds, *Journal of Atmospheric Science*, 34, 1149-1152.
- Volz-Thomas, A., Mihelcic, D., Pätz, H., Shultz, M., Gomišček, B., Lindskog, A., Mowrer, J., Oyola, P., Hanson, K., Schmitt, R., Nielson, T., Eggelov, A., Stordal, F. and Vosbeck, M., 1997, Photochemical ozone production rates at different TOR Sites, In: Hov, Ø., (ed), *Tropospheric Ozone Research*, Germany, Springer, 95-97.
- Wiedinmyer, C., Guenther, A., Estes, M., Strange, I, W., Yarwood, G., and Allen, D, T., 2001, A land use database and examples of biogenic isoprene emission estimates for the state of Texas, USA, *Atmospheric Environment*, 35 6465–6477.
- Wiedinmyer, C., Greenberg, J., Guenther, A., Hopkins, B., Baker, K., Geron, C., Palmer, P. I., Long, B. P., Turner, J. R., Petron, G., Harley, P., Pierce, T., Lamb, B., Westberg, H., Baugh, W., Koerber, M., and Jansenn, M., 2005, Ozarks Isoprene Experiment (OZIE): Measurements and modelling of the ‘isoprene volcano’, *Journal Of Geophysical Research*, 110, D18307, doi:10.1029/2005JD005800.

- Wiedinmyer, C., Tie, X. and Guenther, A., 2006, Future Changes in Biogenic Isoprene Emissions: How Might They Affect Regional and Global Atmospheric Chemistry?, *Earth Interactions*, 10, 1-20.
- Zhang, P., Anderson, B., Barlow, M., Tan, B. and Myneni, R., 2004, Climate related vegetation characteristics derived from MODIS LAI and NDVI, *J. Geophys. Res.*, 109, D20105, doi:10.1029/2004JD004720.
- Zunckel, M., Koosailee, A., Yarwood, G., Maure, G., Venjonoka, K., van Tienhoven, A, M. and Otter, L., 2006, Modelled surface ozone over southern Africa during the Cross Border Air Pollution Impact Assessment Project, *Environmental Modelling & Software*, 21, 911-924.